


# Recent advances in catalyst materials for proton exchange membrane fuel cells


Cite as: APL Mater. 9, 040702 (2021); <https://doi.org/10.1063/5.0045801>

Submitted: 29 January 2021 • Accepted: 08 March 2021 • Published Online: 01 April 2021

 L. Mølmen,  K. Eiler, L. Fast, et al.

## COLLECTIONS

 This paper was selected as Featured

 This paper was selected as Scilight



View Online



Export Citation



CrossMark

## ARTICLES YOU MAY BE INTERESTED IN

[Progress towards lower-cost proton exchange membrane fuel cells](#)

Scilight **2021**, 141110 (2021); <https://doi.org/10.1063/10.0004268>

[An overview of bipolar plates in proton exchange membrane fuel cells](#)

Journal of Renewable and Sustainable Energy **13**, 022701 (2021); <https://doi.org/10.1063/5.0031447>

[Epitaxial ferroelectric oxides on silicon with perspectives for future device applications](#)

APL Materials **9**, 040701 (2021); <https://doi.org/10.1063/5.0039161>



## APL Machine Learning

Machine Learning for Applied Physics  
Applied Physics for Machine Learning

**First Articles  
Now Online!**

# Recent advances in catalyst materials for proton exchange membrane fuel cells

Cite as: APL Mater. 9, 040702 (2021); doi: 10.1063/5.0045801

Submitted: 29 January 2021 • Accepted: 8 March 2021 •

Published Online: 1 April 2021



View Online



Export Citation



CrossMark

L. Mølmen,<sup>1,2</sup>  K. Eiler,<sup>3</sup>  L. Fast,<sup>1</sup> P. Leisner,<sup>2</sup>  and E. Pellicer<sup>3,a)</sup> 

## AFFILIATIONS

<sup>1</sup>Department of Electrification and Reliability, RISE Research Institutes of Sweden, Borås, Sweden

<sup>2</sup>Department of Materials and Manufacturing, Jönköping University, Jönköping, Sweden

<sup>3</sup>Departament de Física, Universitat Autònoma de Barcelona, 08193 Bellaterra, Spain

<sup>a)</sup>Author to whom correspondence should be addressed: [eva.pellicer@uab.cat](mailto:eva.pellicer@uab.cat)

## ABSTRACT

Research on fuel cell technology is constantly gaining importance, while global emission requirements are becoming more and more restrictive. For environmentally neutral proton exchange membrane fuel cells (PEMFCs) to become a competitive technology, sustainable infrastructures need to be established. One of the main showstoppers is the utilization of the rare and therefore costly precious metal Pt as the key element in the electrocatalysis of hydrogen and oxygen. A huge amount of research is done on immensely reducing or even replacing Pt for future PEMFC technology. In this research update, the progress on oxygen reduction reaction catalysts in acidic media over the past two years is reviewed, with special attention to their durability.

© 2021 Author(s). All article content, except where otherwise noted, is licensed under a Creative Commons Attribution (CC BY) license (<http://creativecommons.org/licenses/by/4.0/>). <https://doi.org/10.1063/5.0045801>

## NOMENCLATURE

ADT	accelerated degradation test	MA	mass activity
AEM	anion exchange membrane	MEA	membrane electrode assembly
AEMFC	anion exchange membrane fuel cell	MOF	metal-organic framework
ALD	atomic layer deposition	NG	nanographene
<i>b</i>	Tafel slope	NP	nanoparticle
CB	carbon black	NT	nanotube
CNT	carbon nanotube	NW	nanowire
CNW	carbon nanowire	OCV	open circuit voltage
CV	cyclic voltammetry	ORR	oxygen reduction reaction
DFT	density functional theory	PANI	polyaniline
DOE	U.S. Department of Energy	PEM	proton exchange membrane
$E_{1/2}$	half-wave potential	PEMFC	proton exchange membrane fuel cell
ECSA	electrochemically active surface area	PGM	platinum group metal
FC	fuel cell	RDE	rotating disk electrode
GDL	gas diffusion layer	RGO	reduced graphene oxide
HOR	hydrogen oxidation reaction	RHE	reversible hydrogen electrode
IL	ionic liquid	SA	specific activity
$j_k$	kinetic current density	SAC	single-atom catalyst
LSV	linear sweep voltammetry	STEM	scanning transmission electron microscopy
		TEM	transmission electron microscopy
		ZIF-8	zeolitic imidazolate framework

## I. INTRODUCTION

Proton exchange membrane fuel cell (PEMFC) vehicles are emerging into the commercial market as the drive for zero-emission vehicles increases.<sup>1</sup> However, the cost of the PEMFC is still high, with one of the major cost components being the noble metal catalyst. The rather sluggish oxygen reduction reaction (ORR) at the cathode requires catalysts with a higher surface area and optimized structure in order to minimize the use of platinum group metals (PGMs).

Today, Pt and its alloys are the most commonly used catalysts for PEMFCs at both the anode and the cathode. In 2017, the U.S. Department of Energy (DOE) set the technical target of reaching a total loading of platinum group metals below  $0.125 \text{ mg/cm}^2$  by 2020. Their target activities at 0.9 V vs reversible hydrogen electrode (RHE) are a PGM mass activity (MA) of  $0.44 \text{ A/mg}_{\text{PGM}}$  for PGM catalysts and a current density of  $44 \text{ mA/cm}^2$  for PGM-free catalysts.<sup>2</sup> While the Pt loading can easily be reduced below  $0.05 \text{ mg/cm}^2$  at the anode,<sup>3</sup> the stability and performance of the electrocatalyst at the cathode is critical. In the acidic and oxidizing conditions at the cathode, Pt nanoparticles (NPs) tend to agglomerate and grow, thus losing the surface area. Although some research papers have reached the 2020 goals, commercial fuel cells still operate with around  $0.35 \text{ mg}_{\text{Pt}}/\text{cm}^2$  when used in vehicles.<sup>1</sup>

There are several strategies for improving the cathode catalyst in terms of efficiency and durability (Fig. 1). The size of commercial Pt NPs has already been minimized to 3–6 nm. To further reduce the cost and/or improve the catalytic activity of Pt, research groups are aiming at the shape control of Pt NPs, alloying of Pt, core-shell NP structures with Pt-rich surfaces, and the synthesis of hollow NP structures. The durability can be improved by confining the PGM NPs in a carbon based structure, as well as by making use of different support materials. Recycling of membrane electrode assemblies (MEA) containing PtCo has also shown that the global impact of the catalyst can be reduced by extracting the metals from the aged MEA and synthesizing new catalysts.<sup>4</sup>

On the other hand, Pt-free catalysts such as single-atom catalysts (SAC) are the focus of investigations (Fig. 1). These are most commonly of M–N–C type, where M is a metal, most commonly Fe or Co.<sup>3</sup> Optimization of these catalysts is currently followed up

by creating edge-rich and porous structures, making use of favorable structures such as graphene or carbon nanotubes (CNTs), and by increasing the catalyst's hydrophobicity. Additionally, transition metal dithiolenes (M–S–C structures) comprising Fe or Co have been recently proposed by density functional theory (DFT).<sup>5</sup> A number of different compounds have likewise been determined by DFT as sufficiently stable two-dimensional materials for ORR,<sup>6</sup> although experimental demonstration is yet to be performed.

In the following, the most recently investigated electrocatalysts for ORR will be discussed for each strategy, being split into PGM-based catalysts on the one hand and PGM-free catalysts on the other hand. The focus is on their synthesis, performance, and durability. Due to the vast number of publications in the past two years, the focus lies on those works providing membrane electrode assembly (MEA) tests in fuel cells. Additionally, works on catalyst materials that have not been tested at this level but in the view of the authors present promising performance and applicability in the PEMFC have also been considered. The goal of this work is to give a brief overview of the latest developments and to point out the most promising approaches for future research.

While ORR studies in alkaline media are currently very popular, the focus of this work is on the research dedicated to ORR in acidic media in order to identify suitable materials and synthesis processes for the successful development of PEMFCs. The primary objective does not necessarily lie in outperforming commercial Pt/C, but in achieving high reliability and durability of the catalyst in a cost-efficient synthesis process.

## II. PGM-BASED CATALYSTS

Four different approaches are mainly pursued on PGM-based catalysts: the alloying of Pt or other PGM, the optimization of the pure Pt catalyst, an optimization of the supporting substrate, and the protection of the catalyst in an organic structure. Naturally, these approaches are often combined to acquire superior results.

### A. PGM alloys

PGM alloys allow for reducing the use of the PGM, and electronic properties improving the catalytic activity of the PGM can be

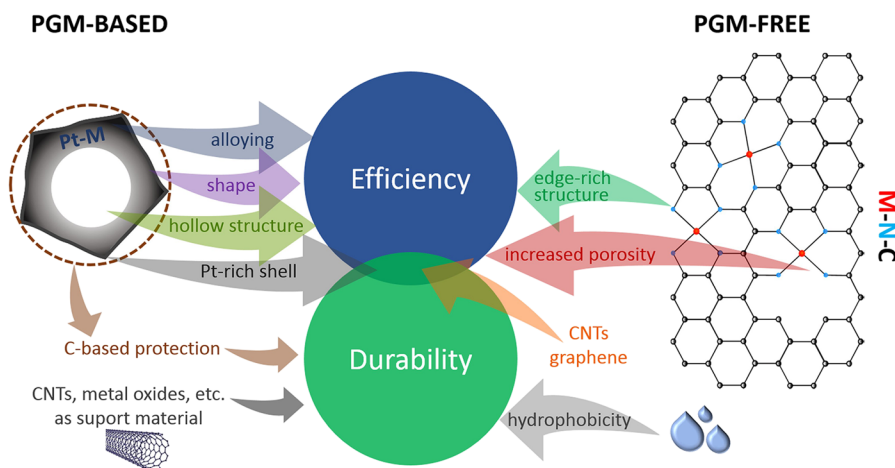


**FIG. 1.** Current strategies for improving the efficiency and durability of PGM-based (left) and PGM-free (right) ORR catalysts for PEMFCs.

obtained. The alloying elements may also contribute with their own catalytic activity.

One of the most popular approaches is the alloying of Pt with transition metals such as Fe, Co, Ni, and Cu, which are usually employed in the form of NPs with a Pt-rich surface. The Pt-rich and electrochemically stable surface is usually formed by either a specific etching process or the dissolution of transition metal atoms during operation; the result is often referred to as a core-shell structure. Several of these catalysts are already being used commercially, such as Pt-Co, which serves in Toyota's fuel cell car;<sup>7</sup> however, research on different Pt-Co NP structures is still ongoing.<sup>8–11</sup> Current research focuses a lot on the development of Pt-Ni alloys,<sup>12–15</sup> where several works report the synthesis of octahedral NPs.<sup>16–20</sup>

Gong *et al.* successfully synthesized Pt-Ni as dumbbell-shaped particles, which did not show increased electrochemically active surface area (ECSA) but were able to achieve both higher ORR MA and higher retention of activity after accelerated degradation testing (ADT) when compared to globular Pt-Ni NPs<sup>21</sup> (Fig. 2).

A neural-like network of Pt-Co NPs connected by CNTs (Fig. 3) developed by Wang *et al.* was able to show outstanding performance at both H<sub>2</sub>/O<sub>2</sub> and H<sub>2</sub>/air fueled PEMFCs while being completely free from degradation after both ADT in an electrochemical half-cell and continuous operation of PEMFC.<sup>22</sup>

Several other binary alloys investigated involve Pt-Ag,<sup>23</sup> Pt-Bi,<sup>24</sup> Pt-Cu,<sup>25,26</sup> Pt-Fe,<sup>27–30</sup> Pt-Ir,<sup>31–35</sup> Pt-Se,<sup>36</sup> Pt-Te,<sup>37</sup> and Pt-Zn.<sup>38</sup> In addition, several ternary<sup>39–48</sup> and quaternary alloys<sup>49,50</sup> have been investigated. A Pt-rare earth catalyst is proposed by Chu *et al.*;<sup>51</sup> however, such a catalyst is questionable in terms of large-scale application due to its low abundance.

Apart from alloying, a few works concentrated on the phosphorization<sup>52,53</sup> or nitrogenation<sup>54</sup> of Pt.

Dionigi *et al.* and Cao *et al.* reported further improvement in the durability of octahedral Pt-Ni by introducing additional alloying elements in a second synthesis step, such as Mo<sup>39</sup> or Cu,<sup>40</sup> respectively.

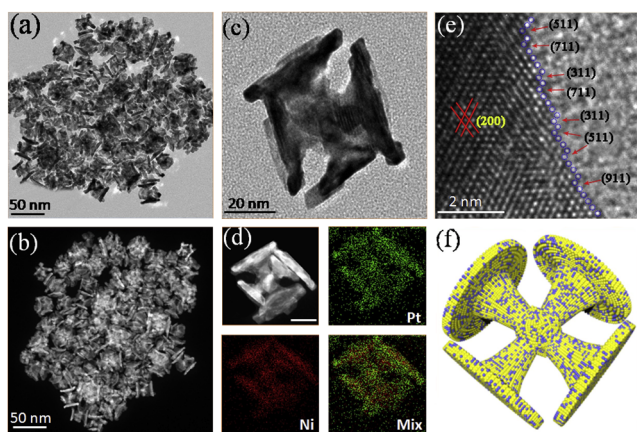


**FIG. 2.** Dumbbell-shaped Pt-Ni NPs for ORR captured by TEM [(a), (c), and (e)], STEM [(b) and (d)], and their 3D structure model (f). The Pt-Ni/C catalyst reached an ORR MA of over 1.3 A/mg<sub>Pt</sub>.<sup>21</sup> Reprinted with permission from Gong *et al.*, Appl. Catal. B **246**, 277 (2019). Copyright 2019 Elsevier.

Wang *et al.* investigated ternary alloys of Pt with the three transition metals Fe, Ni, and Co, finding that the Pt-Co-Fe alloy was the most favorable among the possible combinations in terms of both activity and durability.<sup>43</sup>

The non-platinum containing PGM alloys recently reported for acidic ORR are Pd-based<sup>55,56</sup> or Ir-based.<sup>57</sup> Pd-Mo nanosheets investigated by Luo *et al.* showed extremely high ORR activity in alkaline media and also have superior performance in acidic media; however, the authors considered that the stability in acidic media was insufficient for practical applications.<sup>55</sup> More frequently, Pd is also alloyed with Pt in a variety of nanostructures.<sup>55,58–63</sup> Several works reported ternary alloys including both Pt and Pd.<sup>64–69</sup> Nan *et al.* investigated different Pd-M/Pt core-shell catalysts with Ni, Co, and Fe as alloying elements. The Pd-Fe core provided the best ORR activity, while all alloy cores outperformed the catalyst containing a pure Pd core.<sup>68</sup> A ternary alloy of exclusively noble metals (Pt-Pd-Ir) was investigated by Deng *et al.*<sup>70</sup>

For most reported alloy catalysts, an improvement due to alloying with additional elements is reported. Deng *et al.* found that binary Pt-Pd on carbon nanowires (CNWs) outperformed ternary Pt-Pd-Au, however, the Au phase was mostly segregated so that the effect of alloying could not be studied.<sup>59</sup>

## B. Optimization of pure Pt catalysts

The optimization of pure Pt focuses on shape-tuning, to optimize ECSA and to expose the most active crystal planes, and on the tuning and control of the particle size. In terms of shape, rhombic dodecahedral NPs show the highest activity in perchloric acid, while the cubic shape is the least favorable<sup>71</sup> (Fig. 4).

Dong *et al.* studied the mechanism of ORR on Pt(100), Pt(110), and Pt(111) facets and were able to monitor the intermediates *in situ* by Raman spectroscopy. On Pt(111), where ORR is improved, the reaction takes place via the formation of HO<sub>2</sub> radicals, whereas OH radicals are formed on Pt(100) as well as Pt(110).<sup>72</sup> Chen *et al.* synthesized NPs in a multipod structure showing good performance; however, degradation was still an issue.<sup>73</sup>

Cheng *et al.* used an Se film on the carbon support in order to seed Pt NPs smaller than 2 nm, resulting not only in superior performance but also in much improved durability.<sup>74</sup> Another approach was pursued by Chen *et al.*, who synthesized supramolecular Pt-containing structures with promising results for ORR.<sup>75</sup>

## C. Optimization of the supporting layer

The interface between the PGM catalyst and its supporting layer is crucial since poor adhesion can lead to catalyst detachment. In addition, the support must provide an electrical connection to the catalyst and may influence the density of states in the d-band of the catalyst. Carbon black (CB) is the most commonly used support for the PEMFC catalyst. Current research includes the use of CNTs,<sup>22,76–80</sup> CNWs,<sup>9,59,81</sup> metal oxides,<sup>82–86</sup> a combination of those,<sup>87</sup> and various other compounds.<sup>88–91</sup> Those can be used to either replace CB or act as an intermediate support between the catalyst and CB.

Doping of CB with N, as well as the use of Mn as a precursor results in more graphitic and corrosion-resistant carbon.<sup>92,93</sup> As reported by Yang *et al.*, Pt particles deposited on N-CB were smaller and better dispersed, resulting in an increase in ECSA and

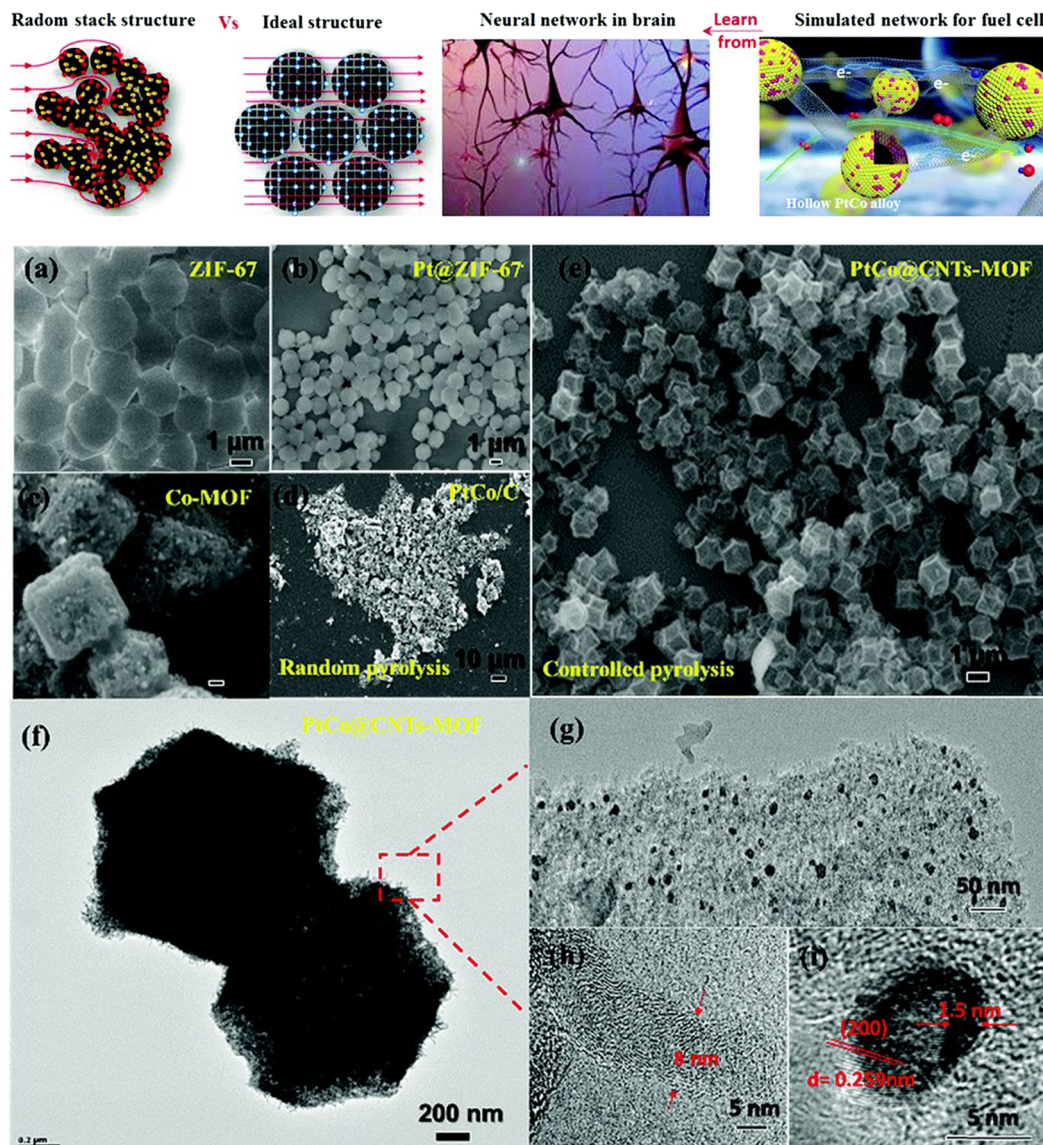


**FIG. 3.** Scheme of hollow Pt–Co NPs in an organic network connected by CNTs inspired by the neural network (top). SEM micrographs of the intermediate products during synthesis [(a)–(c)] and the products after pyrolysis [(d) and (e)]. TEM micrographs of the obtained Pt–Co/CNT/C catalyst [(f)–(i)], which reached a peak power density of over  $1 \text{ W/cm}^2$  in a  $\text{H}_2/\text{O}_2$  PEMFC at a Pt loading as low as  $60 \mu\text{g/cm}^2$  at the cathode.<sup>22</sup> Republished with permission from Wang *et al.*, *J. Mater. Chem. A* 7, 19786 (2019). Copyright 2019 Royal Society of Chemistry.

PEMFC performance.<sup>92</sup> Increased graphitization is also achieved by N-doping along with increased porosity of the carbon support.<sup>93,94</sup> N-doping is proposed to also give a more homogeneous ionomer distribution.<sup>94</sup> Coalescence of Pt and Pt–Co particles was suppressed by utilizing a porous carbon support, resulting in improved performance and durability.<sup>95</sup>

#### D. Protection of the PGM catalyst in an organic matrix

The most promising approach in order to limit degradation and increase the durability of PGM catalysts is their protection in a

carbon-based matrix, where the PGM catalyst is not in direct contact with the polymer membrane.<sup>96,97</sup> Zhao *et al.* successfully “confined”  $\text{Pt}_3\text{Co}$  NPs in mesoporous carbon derived from the zeolitic imidazolate framework (ZIF-8). With the NPs trapped in the mesoporous structure, both detachment and agglomeration of NPs could be largely avoided, while the catalytic activity was not compromised.<sup>98</sup> Li *et al.* used an ionic liquid (IL) film to cover Pt/C NPs. In addition to the protective effect of those films, their electronic properties also improved ORR activity with respect to the bare Pt/C.<sup>99</sup> Zhou *et al.* created a carbon-based shell for Pt derived from Nafion,

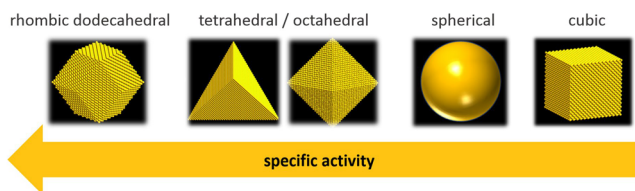


FIG. 4. Shape dependency of ORR activity for pure Pt NPs in perchloric acid.

improving the PEMFC performance at a low Pt loading of 0.07 mg/cm<sup>2</sup>; however, the durability was not studied.<sup>96</sup>

Choi *et al.* synthesized Pt–Fe NPs in a block copolymer matrix and achieved the formation of a carbon shell around the NPs. This catalyst achieved extremely high Pt mass activity in a half cell of 9 A/mg, and in PEMFC, an extremely low Pt loading of 0.01 mg/cm<sup>2</sup> was used to achieve a performance comparable to commercial Pt/C.<sup>30</sup>

Xiao *et al.* investigated the ORR of the noble metals Ir and Ru in a PGM–N–C configuration as SACs, reporting extraordinarily high ORR MAs including promising results at the PEMFC level.<sup>100,101</sup> Liu *et al.* determined that Ir and Rh showed favorable performance when applied as SAC, in contrast to Pt and Pd.<sup>102</sup>

### E. Synthetic strategies

The most common approach for the synthesis of PGM-based catalysts is the solvothermal reduction method in autoclave. Meanwhile, alternative synthesis routes include pyrolysis, galvanic replacement, selective etching, and electrodeposition (Fig. 5). Moreover, the synthesis may comprise those multiple synthesis steps.

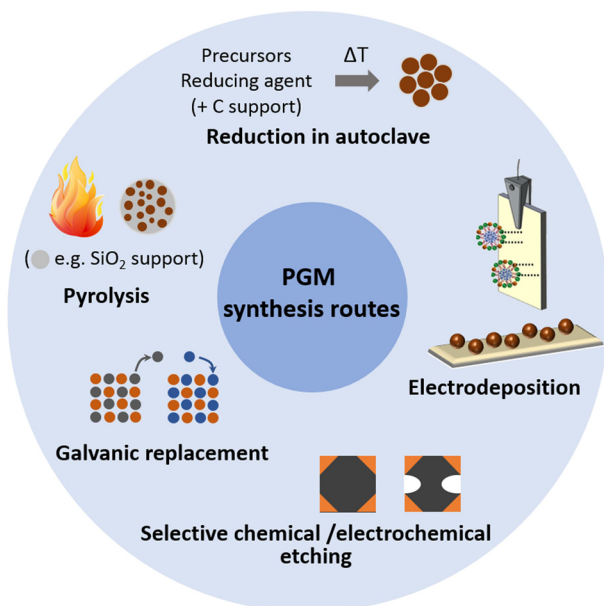


FIG. 5. Main strategies for the synthesis of PGM electrocatalysts.

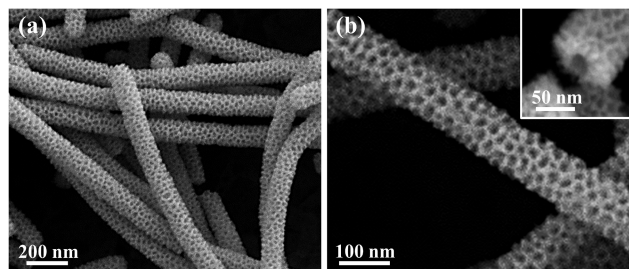


FIG. 6. SEM micrographs of Pt–Co mesoporous NTs synthesized using Te NWs and F127 block copolymer as templates. The inset in (b) shows the cross section of a NT. Interestingly, the Pt–Co NTs outperformed Pt–Ni NTs synthesized through the same route.<sup>106</sup> Reprinted with permission from Yin *et al.*, ACS Sustainable Chem. Eng. 7, 7960 (2019). Copyright 2019 American Chemical Society.

In the solvothermal reduction method, metal precursors (usually acetyl acetates) are dissolved and mixed with a reducing agent and other additives. Carbon is often mixed in before the reduction process, which takes place in an autoclave at elevated temperatures. The product is then dried. For application in an MEA, the catalyst is usually dispersed in a solvent and sprayed onto the electrode.

Zhao *et al.* studied the size dependence of icosahedral Pt NPs synthesized using tetraethylene glycol as both the solvent and reductant and were able to synthesize the catalyst within 20 min. Interestingly, the highest kinetic current was reached for the largest NPs (14 nm), which also exhibited the best durability.<sup>103</sup>

Lei *et al.* demonstrated the synthesis of Pt–Co, Pt–Fe, and Pt–Ni NPs through the same route, allowing a direct comparison between their ORR activities, finding that Pt–Co was the most active at the ORR between them.<sup>104</sup> A similar observation was made by Wang *et al.*<sup>105</sup>

Yin *et al.* reported a room temperature synthesis for mesoporous Pt–Co and Pt–Ni nanotubes (NTs).<sup>106</sup> Here, the reduction of Pt–M (M = Co, Ni) takes place using ascorbic acid as a reducing agent and by galvanic replacement of the previously synthesized Te nanowires (NWs). In addition, a polymeric surfactant introduces mesoporosity in the material (Fig. 6). The same approach is used by the group to prepare mesoporous Pt–Te NTs.<sup>37</sup>

Yang *et al.* proposed a silica-assisted pyrolysis method for the reduction of Fe–Pt NPs.<sup>27</sup> After pyrolysis, the silica is removed and the Pt–Fe NPs are etched to obtain a hollow structure (Fig. 7). Alternative synthesis routes for Pt–Fe NPs are the

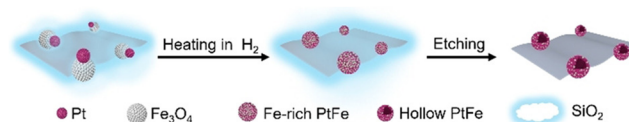
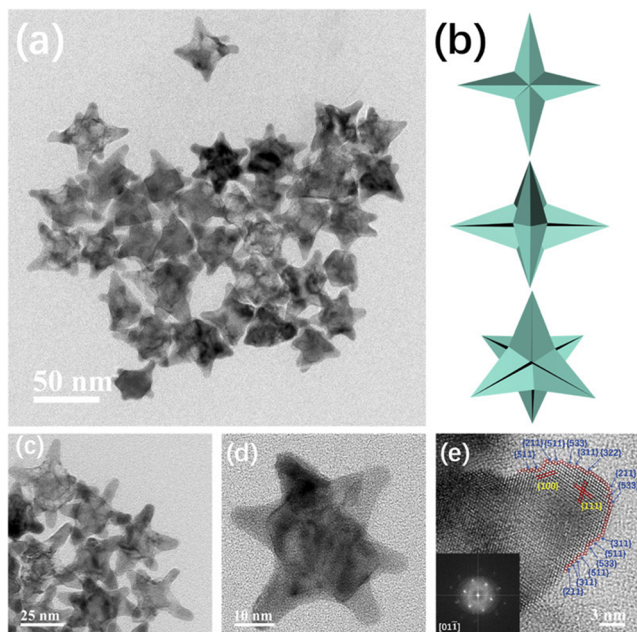


FIG. 7. Scheme for the formation of hollow Pt–Fe NPs from Pt and Fe<sub>3</sub>O<sub>4</sub> precursors by silica-assisted pyrolysis. SiO<sub>2</sub> prevents the agglomeration of NPs during the heat treatment at 900 °C at which formation of Pt–Fe NPs takes place. Subsequent etching in HF removes SiO<sub>2</sub> and dealloys the NPs to obtain an electrochemically stable composition of Pt–Fe. The Pt–Fe/C catalyst reached a MA of over 1 A/mg<sub>Pt</sub> and 91% retention of MA after ADT.<sup>27</sup> Reprinted with permission from Yang *et al.*, Chem. Eur. J. 26, 4090 (2020). Copyright 2019 Wiley-VCH Verlag GmbH & Co. KGaA, Weinheim.



**FIG. 8.** TEM micrographs [(a) and (c)–(e)] and 3D model (b) of hexapod Pt–Pd–Cu NPs, which reached an ORR MA of  $1.17 \text{ A/mg}_{\text{Pt}}$ .<sup>64</sup> Reprinted with permission from Chen *et al.*, ACS Sustainable Chem. Eng. **8**, 1520 (2020). Copyright 2020 American Chemical Society.

impregnation–reduction method<sup>28</sup> and pyrolysis from a single precursor.<sup>29</sup> Higher process temperatures lead to the formation of an ordered structure, more favorable for ORR activity.<sup>28,29</sup>

Chen *et al.* achieved the synthesis of ternary Pt–Pd–Cu alloy NPs in a hexapod shape (Fig. 8). The formation of this unique shape was triggered by a combination of etching and selective growth.<sup>64</sup>

Mesoporous structures are reported in many cases, and their catalytic activity is certainly promising due to their generally higher

ECSA and MA.<sup>17,37,65,67,69,70,106</sup> However, their applicability in a PEMFC is questionable, as its performance depends on the number of triple points, which do not necessarily increase due to mesoporosity of the catalyst. In these cases, high ORR activities at the rotating disk electrode (RDE) level need to be backed up by PEMFC testing to prove the effect of a mesoporous structure on the FC. Otherwise, porous structures can still lead to improved MAs due to a decrease in the amount of non-surface material and can be ultimately optimized by the synthesis of hollow structures, as long as the stability is not compromised.<sup>12,27,69</sup>

A more promising approach is the combination of the catalyst with a mesoporous support layer, where the catalyst is confined within the mesopores.<sup>94,98,107</sup>

An alternative for the synthesis of PGM NPs is through pulse electrodeposition onto the carbon support.<sup>11,108</sup> Wang *et al.* successfully deposited Pt NPs within a desirable particle size of 3–10 nm after determining the optimum deposition parameters. The electrodeposited Pt/C showed higher half-wave potential  $E_{1/2}$ , kinetic current density  $j_k$ , and stability with substantially lower Pt loading in comparison to commercial Pt/C.<sup>108</sup>

Hussain *et al.* produced an Nb–Ti oxide substrate by atomic layer deposition (ALD), followed by the deposition of Pt by magnetron sputtering, and high ORR activity at a very low Pt loading of  $9 \mu\text{g}/\text{cm}^2$  was reached.<sup>86</sup> A sputter deposition approach was also followed by Ergul-Yilmaz *et al.* for the deposition of Pt.<sup>109</sup>

## F. Durability issues

Many PGM-based catalysts suffer from constant performance degradation.<sup>12</sup> For pure Pt, this generally refers to the dissolution and redeposition of Pt, leading to particle growth and thus loss of the total catalyst area.<sup>110</sup> For alloys, leaching of non-noble metals can cause compositional and structural changes. A detailed *in situ* examination of the degradation of octahedral Pt–Ni was performed by Beermann *et al.*, identifying coalescence and particle motion as the main degradation mechanisms.<sup>111</sup> Another considerable problem of pure Pt is its methanol-dependent performance.

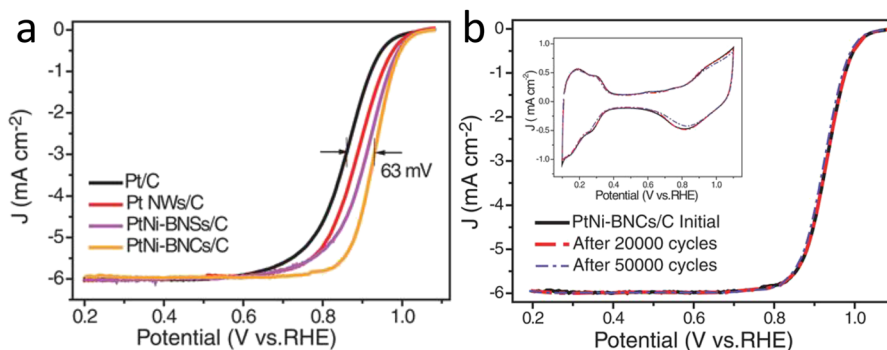


**FIG. 9.** Comparison of linear sweep voltammograms (LSVs) of C-supported Pt–Ni bunched nanocages (PtNi–BNCs/C), Pt–Ni bunched nanospheres (PtNi–BNSs/C), Pt NWs, and commercial Pt/C, where the Pt–Ni nanocages demonstrate an improvement of 63 mV in  $E_{1/2}$  with respect to commercial Pt/C (a). LSVs of C-supported Pt–Ni nanocages including cyclic voltammograms (inset) initially and after 20 000 and 50 000 cycles of ADT, showing that neither ORR nor ECSA is significantly affected by the ADT (b).<sup>12</sup> Reprinted with permission from Tian *et al.*, Science **366**, 850 (2019). Copyright 2019 AAAS.

**TABLE I.** Characteristics of ORR for different PGM-based electrocatalysts in 0.1 M HClO<sub>4</sub>.  $j_k$ , MA, and SA are given at 0.9 V vs RHE. ADT refers to 10 000 potential cycles between 0.6 and 1.0 V unless stated otherwise. MA and ECSA usually refer to Pt mass only. All potentials refer to RHE.

Catalyst	Kinetic current density $j_k$ (mA/cm <sup>2</sup> )	Half-wave potential $E_{1/2}$ (V)	Tafel slope $b$ (mV/dec)	Mass activity MA (mA/mg)	Specific activity SA (mA/cm <sup>2</sup> )	Electrochemical surface area ECSA (m <sup>2</sup> /g)	Retained mass activity after ADT (%)	Loss in $E_{1/2}$ after ADT (mV)	References
Ir-N-C	9.8	0.86	41	12 200 <sup>a</sup>				n/a <sup>b</sup>	100
Ir-N-C		0.83	48				97 <sup>c</sup>		102
Na-Pt-R/C		0.71	118					35 <sup>d</sup>	75
Pd-Mo/C				660 <sup>a</sup>	0.47	139			55
Pt/C		0.95		2 070	3.1	70	97		114
Pt/C				870	1.49				119
Pt/C				370	0.55	69	58		73
Pt/C				860	0.99	87	83 <sup>e</sup>		115
Pt/C	3.4	0.91							108
Pt/C		0.88				44		27	81
Pt/C				260	0.43	69			96
Pt/C				260	0.65	40	74 <sup>f</sup>		109
Pt(N)/C		0.93		102		69	96 <sup>g</sup>		54
Pt/C-N	3.13	0.87	98					5 <sup>h</sup>	120
Pt/C/PANI				63	0.09				121
Pt/Co-N/C		0.89		227		48	85 <sup>h</sup>	4 <sup>h</sup>	10
Pt/Ir/C	2.9	0.86		373	1.30		84 <sup>b</sup>		33
Pt/Mn/C		0.88		300	0.57	67		31 <sup>h</sup>	93
Pt/Se/C		0.96		750	0.32	231	93		74
Pt/IL/C				800	1.32				99
Pt/Nb-O/C		0.92	64	560	0.85	66	100		84
Pt/Nb-O/C				429	0.52	83	80 <sup>i</sup>		83
Pt/Nb-O/CNT <sup>l</sup>	1.1	0.86	59	57		82	93 <sup>h</sup>	6 <sup>h</sup>	87
Pt/Nb-Ti-O/C <sup>j</sup>		0.77	52	56	0.32			20	86
Pt/Pd/C				750	1.01		60		62
Pt/Pd-Co/C				160 <sup>a</sup>	0.58	130			68
Pt/Pd-Fe/C				260 <sup>a</sup>	0.88	129	89		68
Pt/Pd-Ni/C				110 <sup>a</sup>	0.69	125			68
Pt/Ti-C		0.82		80	0.13		88	1	88
Pt/Ti-N		0.85		140	0.27		79	7	88
Pt/Ti-Nb-O				150	0.35	43			82
Pt/Ti(N,C)O				115		41	n/a		85
Pt/Ti-C-O(F)/CNT		0.90		210	0.32	64			79
Pt/Ti-C-O(F)/CNT		0.88		163	0.26	63		19 <sup>k</sup>	80
Pt/Pd/W-Ni/C		0.90		370 <sup>a</sup>			n/a <sup>h</sup>	1 <sup>h</sup>	90
Pt-Ag/C	2.17	0.88		316	3.46	91	n/a		23
Pt-Au-Cu/C		0.92	78	750 <sup>a</sup>	0.49	153		n/a	48
Pt-Bi/C		0.84		1 040			87 <sup>c</sup>		24
Pt-Co/C		0.97		2 260	8.6	27	94 <sup>l</sup>		8
Pt-Co/C			151	128		30	78 <sup>d</sup>		26
Pt-Co/C		0.89		640	1.29	49	86		104
Pt-Co/C				740	1.74		91	5	105
Pt-Co/C		0.91	62	950	0.99	50			106
Pt-Co/Nb-O/C				449	0.63	71	n/a		83
Pt <sub>3</sub> Co/C		0.93	62	830	1.44	58	87 <sup>b</sup>	5 <sup>b</sup>	98
Pt-Co/CNT		0.94		852	1.38	62	103	n/a	22
Pt-Co-Fe/C		0.90		650		26	84	6	43
Pt-Co-Ni-Mo/C				450		49	78		49
Pt-Cu/C				2 570	2.82	91			25



TABLE I. (Continued.)

Catalyst	Kinetic current density $j_k$ (mA/cm <sup>2</sup> )	Half-wave potential $E_{1/2}$ (V)	Tafel slope $b$ (mV/dec)	Mass activity MA (mA/mg)	Specific activity SA (mA/cm <sup>2</sup> )	Electrochemical surface area ECSA (m <sup>2</sup> /g)	Retained mass activity after ADT (%)	Loss in $E_{1/2}$ after ADT (mV)	References
Pt-Cu-Ni/C				1 290	1.7	73	93 <sup>m</sup>	10 <sup>m</sup>	46
Pt-Cu-Ni-W/C				2 020		126	66 <sup>g</sup>		50
Pt-Cu-W/C		0.93	56	750	1.43	53	96 <sup>h</sup>		42
Pt-Fe/C		0.92	58	680	2.23	30	73		28
Pt-Fe/C				300		54			29
Pt-Fe/C			48	1 020	2.73	37	91		27
Pt-Fe/C		0.88		470	0.92	51	74		104
Pt-Fe/C						50			92
Pt-Fe/C				9 000			69		30
Pt-Fe/TiCrN				674	1.28		90 <sup>b</sup>	6 <sup>b</sup>	107
Pt-Fe-Mo/C		0.92		780	0.56	133	67 <sup>m</sup>	26 <sup>m</sup>	47
Pt-Ir/C		0.87			1.18	32		23	32
Pt-Ir/C		0.91	65	522 <sup>a</sup>	1.56	33		30 <sup>b</sup>	35
Pt-Ir@Pd/C				1 880	1.27	122 <sup>n</sup>	84		31
Pt-Ni/C				1 640		38	63		39
Pt-Ni/C		0.94		1 676	5.84	29			16
Pt-Ni/C		0.93		1 330		27	73		21
Pt-Ni/C				914	2.45	37	75 <sup>o</sup>	14 <sup>o</sup>	17
Pt-Ni/C			58	1 900	7.7	25	91 <sup>b</sup>	5 <sup>b</sup>	18
Pt-Ni/C				790		30	58 <sup>p</sup>		19
Pt-Ni/C			54	3 520	5.16	68	99 <sup>e</sup>		12
Pt-Ni/C	2.84	0.87	26	268	14.3	19			13
Pt-Ni/C		0.87		400	0.77	52	70		104
Pt-Ni/C		0.90	61	900	0.89	49			106
Pt-Ni/C						45			92
Pt-Ni/C				14		29			14
Pt <sub>3</sub> Ni(Au)/C				3 080	5.74	35	95 <sup>g</sup>		113
Pt-Ni/Nb-O/C				539	0.50	107	n/a		83
Pt-Ni-Cu/C				3 700	6.2	60	82 <sup>m</sup>		40
Pt-Ni-In/C				760	1.96	39	98 <sup>q</sup>		41
Pt-Ni-Ir/C				409		85	86 <sup>b</sup>		45
Pt-Ni-Mo/C				3 430		38	72		39
Pt-P/C		0.93		915	1.86	52	93		52
Pt-Pd/C						70			92
Pt-Pd/C				920 <sup>r</sup>	1.04	72 <sup>r</sup>	91 <sup>p</sup>	9 <sup>p</sup>	58
Pt-Pd/C		0.87		411	0.43	93	88 <sup>b</sup>		59
Pt-Pd/C		0.92		850 <sup>a</sup>	1.33	54	73	14	60
Pt-Pd/C				480 <sup>a</sup>	1.93	45	54 <sup>m</sup>	30 <sup>m</sup>	61
Pt-Pd/C		0.90	65	410 <sup>a</sup>	0.91	52		20 <sup>b</sup>	35
Pt-Ir/C				31 <sup>a</sup>		57			34
Pt-Pd-Ag/C		0.90	59	610	1.11	55		11 <sup>b</sup>	65
Pt-Pd-Cu/C		0.93		1 170	2.20	53	63	12	64
Pt-Pd-Ir/C		0.95	63	1 030	2.08	48	78	7	70
Pt-Pd-Ni/C		0.94	68	1 140	1.52	56		n/a	69
Pt-Pd-Ni/C			77	1 170	3.8	32	84		66
Pt-Pd-Ni-P/C		0.93	61	450	0.89	51	84	6 <sup>b</sup>	67
Pt-Te/C		0.92	65	400	0.9	45	92 <sup>s</sup>		37
Pt-Y-O/C				108	0.20	53	83 <sup>o</sup>		51
Pt-Zn/C		0.94		1 020	1.68	61		n/a	38
Rh-N-C		0.68	51						102

TABLE I. (Continued.)

Catalyst	Kinetic current density $j_k$ (mA/cm <sup>2</sup> )	Half-wave potential $E_{1/2}$ (V)	Tafel slope $b$ (mV/dec)	Mass activity MA (mA/mg)	Specific activity SA (mA/cm <sup>2</sup> )	Electrochemical surface area ECSA (m <sup>2</sup> /g)	Retained mass activity after ADT (%)	Loss in $E_{1/2}$ after ADT (mV)	References
Ru–N–C		0.82	54	4 780 <sup>a</sup>	11.95			17 <sup>g</sup>	101
Se/Pt/C		0.82 <sup>h</sup>	58		1.7				36

<sup>a</sup>Normalised by total PGM mass.

<sup>b</sup>After 5000 potential cycles of ADT.

<sup>c</sup>After 10 000 seconds of chronoamperometry.

<sup>d</sup>After 1000 potential cycles of ADT.

<sup>e</sup>After 50000 potential cycles of ADT.

<sup>f</sup>After 3000 potential cycles of ADT.

<sup>g</sup>After 20000 potential cycles of ADT.

<sup>h</sup>After 30000 potential cycles of ADT.

<sup>i</sup>After 25000 potential cycles of ADT.

<sup>j</sup>In H<sub>2</sub>SO<sub>4</sub>.

<sup>k</sup>After 2000 potential cycles of ADT.

<sup>l</sup>At 60 °C.

<sup>m</sup>After 15000 potential cycles of ADT.

<sup>n</sup>Normalized by mass of Pt and Ir.

<sup>o</sup>After 6000 potential cycles of ADT.

<sup>p</sup>After 8000 potential cycles of ADT.

<sup>q</sup>After 4000 potential cycles of ADT.

<sup>r</sup>Normalized by total catalyst mass.

<sup>s</sup>After 5 h of chronoamperometry.

<sup>t</sup>Recalculated from Ag/AgCl assuming a pH of 1.

Mom *et al.* investigated the oxidation behavior of Pt under PEMFC conditions and found that oxidation of Pt was favored under wet conditions at oxidizing potentials, especially on Pt NPs. Furthermore, the authors showed that the use of a Br-containing membrane instead of a regular Nafion membrane could suppress oxide formation.<sup>112</sup>

Outstanding durability has been reported by Tian *et al.* on bunched Pt–Ni nanocages, with only marginal decrease in MA after 50 000 cycles of ADT (Fig. 9). This performance has been related to the protective Pt skin structure of the catalyst.<sup>12</sup> Wu *et al.* improved the durability of Pt<sub>3</sub>Ni NWs by Au doping, while the ORR activity was unaffected by the addition of Au.<sup>113</sup> Corroborated by DFT studies, the authors suggest that Au occupies surface defects of the Pt<sub>3</sub>Ni matrix and immobilizes Ni atoms. A similar observation was made by Shen *et al.* using In in order to limit the diffusion of Ni.<sup>41</sup> Although the initial performance was inferior to that of a Pt–Ni alloy, an improved durability of Pt–Ni–In was found, and the optimum In content is the result of a trade-off between activity and durability.

Feng *et al.* produced Pt–Te nanosheets, which were then submitted to electrochemical dissolution of Te. The so-obtained porous Pt nanosheets showed very high MA and durability even after 30 000 potential cycles.<sup>114</sup> Similar observations were made by Kong *et al.* after dealloying Pt–Ni NWs<sup>115</sup> and referred to the higher defect density of dealloyed Pt, leading to improved ORR performance.<sup>116</sup>

In a different approach, a significant improvement was made by Guo *et al.* to Pt/C by applying a phosphorization treatment, leading to the formation of Pt<sub>2</sub>P.<sup>52</sup>

Tu *et al.* found that the addition of W to Pt–Cu led to the outstanding stability of the catalyst after 30 000 potential cycles, even though the performance has been notably decreased after 5000 cycles.<sup>42</sup> This example shows that sufficiently long durability tests are indispensable for the evaluation of an ORR catalyst and 10 000 potential cycles, as suggested by the DOE, should be the absolute minimum.<sup>2</sup>

The fact that MA of the PGM-based catalysts is often reported with respect to Pt mass leads to the questionable assumption that ORR solely takes place on Pt atoms. Especially, if other PGM-metals such as Pd or Ir are involved, but also in the case of alloying of Pt with non-noble elements, their contribution to ORR activity is neglected and unrealistically high MA are reported. Although the Pt MA is therefore little meaningful from a scientific viewpoint, it can give a good estimation on the required amount of Pt and therefore the cost efficiency. From a purely electrochemical view, the ECSA-normalized specific activity (SA) should provide better comparability (Table I). A sound guidance for measuring and reporting the catalytic activity was produced by Wei *et al.*<sup>117</sup>

Zalitis *et al.* targeted the issue that although Pt alloys often show higher activity around the half-wave potential, they often do not exhibit as high current densities at higher ORR overpotential, close to the working potential of the PEMFC.<sup>118</sup> It is therefore important to document the MA at a higher potential such as 0.9 V vs RHE.

Ir-based catalysts<sup>57</sup> and Pt–Pd alloys<sup>35</sup> show very good CO tolerance in contrast to Pt. Bak *et al.* further found that carbon corrosion was suppressed when Ir was present.<sup>34</sup>

### III. PGM-FREE CATALYSTS

Research on PGM-free catalysts for the ORR in acidic media includes ceramic catalysts such as  $\text{CoS}_2$ ,<sup>122</sup>  $\text{NiN}$ ,<sup>123</sup> and  $\text{Fe}_3\text{C}$ ,<sup>124</sup> however, the majority of the PGM-free catalysts are carbon-based. Carbon-based electrocatalysts profit from the huge abundance of carbon as well as from the highly advanced existing technologies able to tune carbon to the desired electronic properties. Carbon

doped with elements such as nitrogen,<sup>125,126</sup> sulfur, phosphorous, and their combinations<sup>127–129</sup> has proven to work as ORR catalysts in both half-cell and PEMFC experiments. However, the current densities of these catalysts are not comparable to their PGM counterparts yet. Therefore, co-doping carbon with nitrogen and a transition metal to form SAC M–N–C structures where  $M=(\text{Fe}, \text{Co}, \text{Cr}, \text{Ni}, \text{Mn}, \text{Ti}, \text{Zn})$ <sup>130–135</sup> is the focus of current PGM-free research.

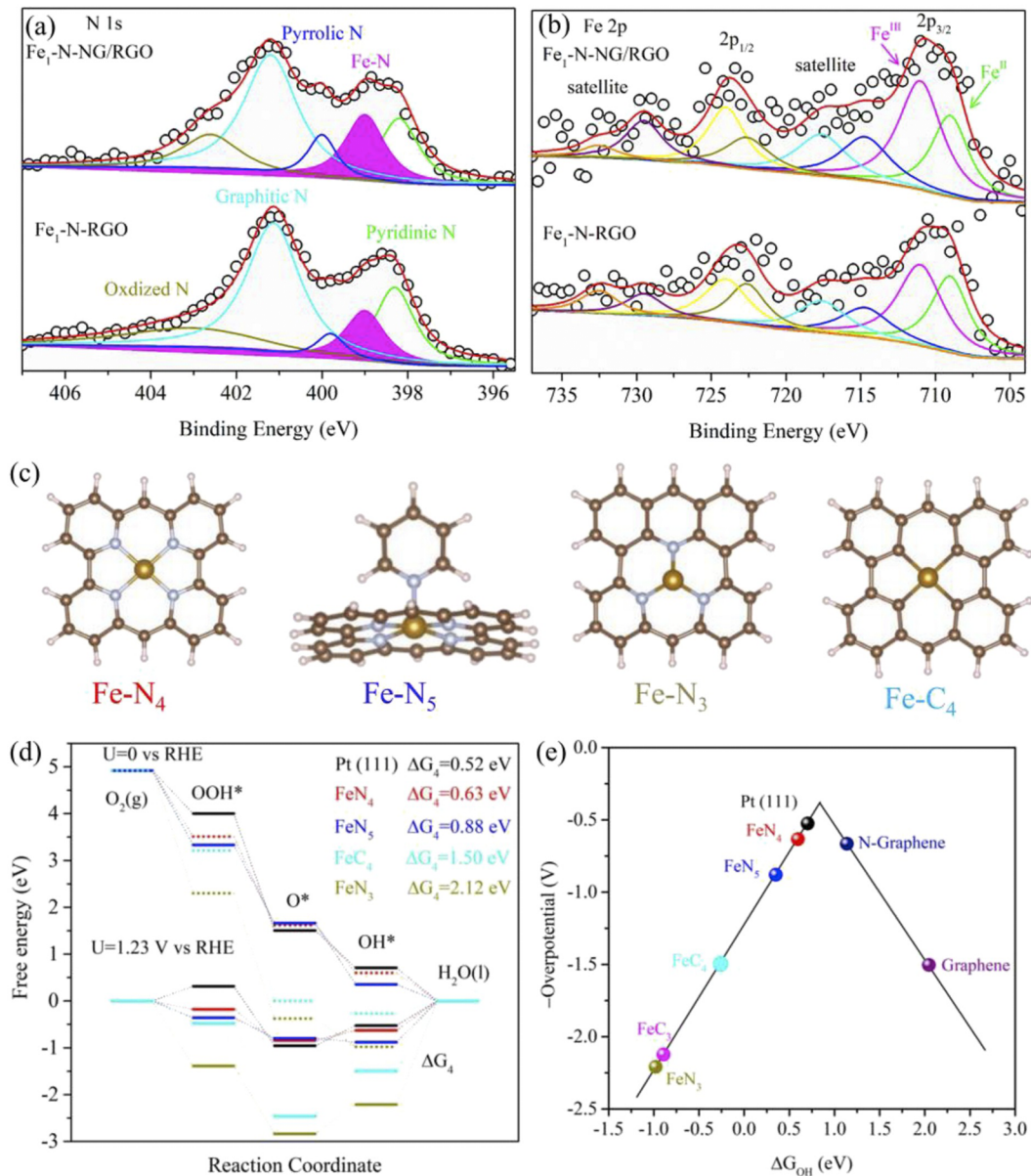


**FIG. 10.** X-ray photoelectron spectra of single-atom Fe anchored to nanographene (NG) and reduced graphene oxide [(RGO), (a) and (b)] and schematic of the  $\text{Fe-N}_4$ ,  $\text{Fe-N}_5$ ,  $\text{Fe-N}_3$ , and  $\text{Fe-C}_4$  active sites where Fe is indicated in gold, N is indicated in gray, and C is indicated in dark orange (c). The free-energy diagram of these sites also at the Pt(111) facet in acidic media from DFT calculations (d) and a volcano plot of the ORR activity by plotting the overpotential as a function of the binding energy of OH of these sites, Pt(111), nitrogen-doped graphene, and graphene (e).<sup>146</sup> Reprinted with permission from Chen *et al.*, *Nano Energy* **66**, 104164 (2019). Copyright 2019 Elsevier.

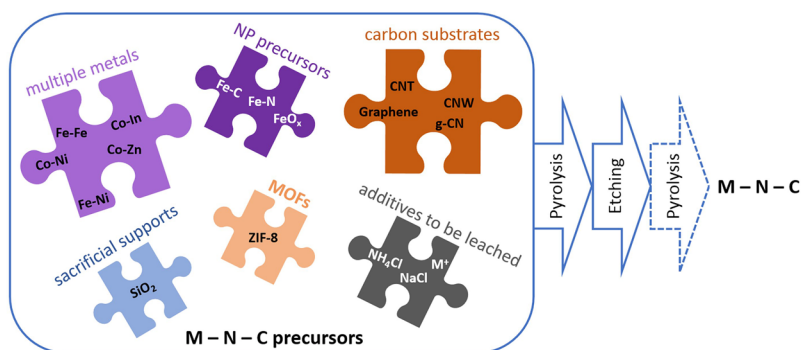


FIG. 11. Scheme for the synthesis of SAC electrocatalysts.

These SACs utilize abundant materials and thus have the potential to significantly reduce the cost of PEMFCs. The electrocatalytic activity of these materials is highly dependent on the type of metal and is reported to follow the order  $\text{Fe} > \text{Co} > \text{Mn} > \text{Cu} > \text{Ni}$ .<sup>136</sup> Fe has therefore been studied extensively.<sup>130,137–144</sup> To facilitate the optimization of SACs, studies to understand which are the active sites have been performed. Zhang *et al.* found pyrrole-type FeN<sub>4</sub> to be most active through both DFT calculations and from high open circuit voltage (OCV) and peak power density from tests in PEMFC. Chen *et al.* reached the same conclusion<sup>145</sup> (Fig. 10). Mun *et al.* investigated the effect of the carbon support on the activity of FeN<sub>4</sub> and found that the activity can be tuned by adding electron-withdrawing/donating groups.<sup>146</sup>

### A. Synthetic strategies

The synthesis of M-N-C catalysts is most commonly done through pyrolysis, where nitrogen containing the organic precursor and metal precursor are mixed and subsequently heated in an inert atmosphere.<sup>138,147,148</sup> Some research groups add sulfur to the M-N-C to improve catalyst activity.<sup>149–152</sup> To ensure porosity, a sacrificial support may be added<sup>147,153–157</sup> or a metal-organic framework (MOF) such as ZIF-8 can be used as the organic precursor.<sup>148,158–163</sup> In principle, several different precursors may be combined (Fig. 11). Zhu *et al.* combined the use of a sacrificial polystyrene template and ZIF-8 to obtain a hierarchically porous structure.<sup>164</sup> The first pyrolysis step is followed by

etching to remove the support, surface oxides, and unstable metal clusters<sup>138,147,148</sup> (Fig. 12). An additional pyrolysis step ensures carbonization and yields a more uniform morphology.<sup>147,148</sup> Several groups have added excess Fe to form NPs of iron carbides or nitrides within the Fe-N-C.<sup>141,165,166</sup>

Gao *et al.* combined the pyrolysis and etching step by adding H<sub>2</sub> to atmosphere during pyrolysis of a MOF-based catalyst. Tunable hierarchical porosity was obtained.<sup>131</sup> Li *et al.* added additional metal ions to the pyrolysis. The metal ions were oxidized during heat treatment and ensured increased porosity while being easily removed during subsequent acid leaching.<sup>154</sup> A hierarchically open-porous structure has been obtained by the addition of graphitic carbon nitride to ZIF-8 and iron precursor prior to pyrolysis.<sup>139,167,168</sup>

Similarly, ammonium chloride or sodium chloride has been added to the pyrolysis to achieve an edge rich structure with more accessible active sites.<sup>149,169</sup> Wang *et al.* also achieved an edge rich structure by using iron chloride as a precursor, and both experiments and DFT calculations showed higher catalytic activity of the Fe-N<sub>x</sub> sites at edges compared to those at the center of the carbon matrix.<sup>138</sup> Another strategy is to increase the density of active sites as done by Wan *et al.* by making concave structures.<sup>142</sup>

Wang *et al.* produced iron oxide NPs in a mesoporous N-doped carbon, which after pyrolysis formed a core-shell structure with iron oxide encapsulated in graphitic carbon, and x-ray photoelectron spectroscopy analysis showed Fe-N active sites.<sup>170</sup>

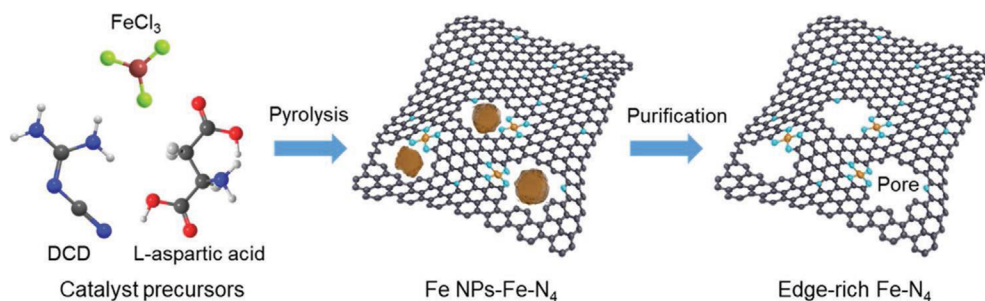
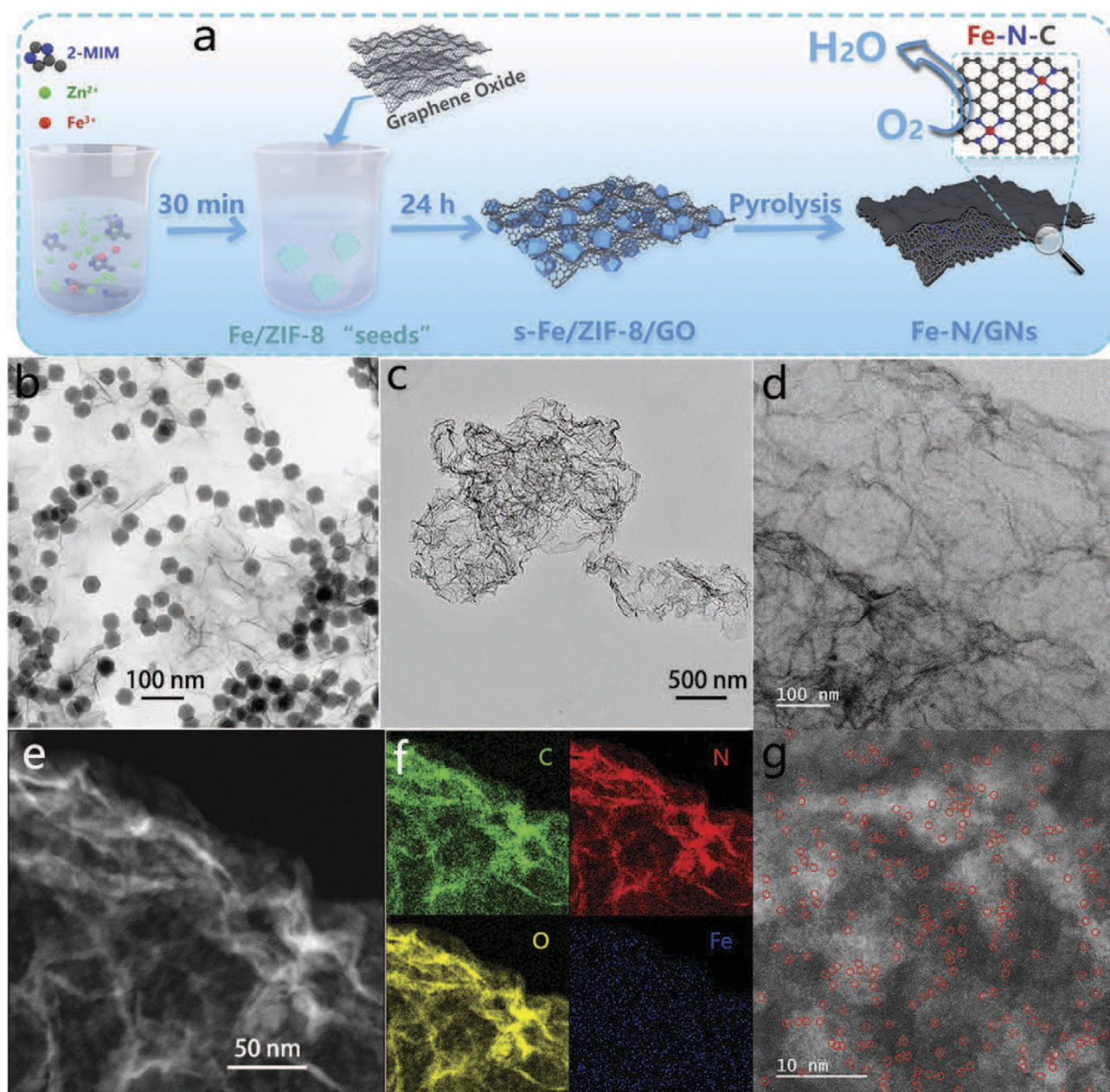


FIG. 12. Formation of Fe-N-C by pyrolysis using L-aspartic acid, dicyandiamide (DCD), and FeCl<sub>3</sub> as precursors.<sup>138</sup> Reprinted with permission from Wang *et al.*, Adv. Mater. **32**, 2000966 (2020). Copyright 2020 WILEY-VCH Verlag GmbH & Co. KGaA, Weinheim.

As an alternative to the pyrolysis of MOF and sacrificial support, Wang and Berthon-Fabry synthesized Fe-N-C using the sol-gel method to produce an aerogel.<sup>171</sup>

Highest performance is, however, found for Fe-N-C catalysts using CNTs and/or graphene as the carbon precursor, with the advantage of not needing a sacrificial support.<sup>172</sup> Li *et al.*

fabricated carbon nanospheres connected with CNTs to improve the electrical conductivity of the catalyst.<sup>173</sup> Liu *et al.* also anchored Fe single atoms on CNTs<sup>174</sup> but further improved the performance by exchanging CNTs for graphene<sup>175</sup> (Fig. 13). The highest performance and durability of a PGM-free catalyst were achieved by Chen *et al.* through supporting NG doped with



**FIG. 13.** Scheme of Fe-N-graphene synthesis (a), TEM image of the intermediate Fe/ZIF-8/graphene oxide (b), TEM and STEM images of the Fe-N-graphene [(c)–(e), and (g)], and elemental mapping of the final product (f).<sup>175</sup> Reprinted with permission from Liu *et al.*, *Small Methods* 4, 1900827 (2020). Copyright 2020 WILEY-VCH Verlag GmbH & Co. KGaA, Weinheim.

**TABLE II.** Characteristics of the ORR for different PGM-free electrocatalysts. ORR was performed in 0.1 M HClO<sub>4</sub> unless stated otherwise. MA and SA are given at 0.8 V. All ECSA were determined by the H<sub>upd</sub> method. ADT refers to 10 000 cycles between 0.6 and 1.0 V unless stated otherwise. All potentials refer to RHE.

Catalyst	Kinetic current density $j_k$ (mA/cm <sup>2</sup> )	Half-wave potential $E_{1/2}$ (V)	Tafel slope $b$ (mV/dec)	Mass activity MA (mA/mg)	Specific activity SA (mA/cm <sup>2</sup> )	Electrochemical surface area ECSA (m <sup>2</sup> /g)	Retained current density after ADT (%)	Loss in $E_{1/2}$ after ADT (mV)	References
C(N,S)		0.74	60				78 <sup>a</sup>		128
C(P,N) <sup>b</sup>	0.96 at 0.5 V								127
N-C		0.76					91 <sup>c</sup>		125
N-C		0.61	108				87 <sup>d</sup>		126
N-P-S-C		0.64	126				84 <sup>a</sup>		129
Co-In-C-N <sup>b</sup>		0.7					79 <sup>a</sup>		180
Co-S			62						122
Co-N-C <sup>b</sup>		0.63						15 <sup>e</sup>	177
Co-N-C <sup>b</sup>		0.84						40 <sup>f</sup>	176
Co-N-C <sup>b</sup>		0.69	48				99 <sup>g</sup>		178
Co-S-N-C	5.53 at 0.5 V	0.68					91.7 <sup>a</sup>		152
(Co,Ni)-C		0.34	104				87 <sup>c</sup>		181
(Co,Zn)-N-CNW		0.80	82					12	182
(Co,Zn)-N-S-C <sup>b</sup>		0.70					85 <sup>d</sup>		150
(Co,Zn)-N-C		0.80						n/a	183
Cr-N-C	24 at 0.75 V	0.77	37					15 <sup>h</sup>	132
Fe-N-C	5.8 at 0.3 V	0.76							137
Fe-N-C		0.82							142
Fe-N-C <sup>b</sup>		0.75					82 <sup>d</sup>		139
Fe-N-C		0.78	65				67 <sup>d</sup>		167
Fe-N-C		0.78					90 <sup>i</sup>		130
Fe-N-C		0.78		10.5	0.0135		75 <sup>j</sup>		140
Fe-Fe <sub>3</sub> C/C		0.73	38					27 <sup>f</sup>	141
Fe-N-C	37 at 0.75 V	0.8	68				n/a <sup>e</sup>		138
Fe-N-C <sup>b</sup>		0.8	72		6.89 <sup>k</sup>			26	143
Fe-N-C		0.81 <sup>b</sup>		6.50			45	53	144
Fe-N-C	6.12 at 0.8 V	0.81	63					18	131
Fe-N-C		0.73				503		19 <sup>l</sup>	145
Fe-N-C		0.74	59					38	162
Fe-N-C		0.81						16	163
Fe-N-C	6.14 at 0.8 V	0.80						n/a	157
Fe-N-C <sup>b</sup>	3.82 at 0.8 V	0.80	65						169
Fe-N-C <sup>b</sup>		0.84						31 <sup>f</sup>	158
Fe-N-C	4.6 at 0.8 V	0.80	66					9	172
Fe-N-C <sup>b</sup>	0.925 at 0.8 V	0.81	75					17	165
Fe-N-C		0.84	73					n/a <sup>a</sup>	175
Fe-N-C		0.79					90.8 <sup>h</sup>		168
Fe-N-C		0.76						10 <sup>f</sup>	156
Fe-N-C		0.79	72				91 <sup>a</sup>		159
Fe-N-C <sup>b</sup>		0.82	92					1	160
Fe-N-CNW	8.0 at 0.8 V	0.82	63					16	154
Fe-N-C/CNT	13.1 at 0.8 V	0.84	67			565		15 <sup>e</sup>	173
Fe-N-CNT		0.73						28	174
Fe-Fe <sub>3</sub> C/Fe-N-C <sup>b</sup>	0.56 at 0.85 V	0.79							166
Fe <sub>2</sub> -N-C <sup>b</sup>	16.4 at 0.75 V	0.78	83					20 <sup>h</sup>	184
Fe <sub>2</sub> N <sub>6</sub> -C <sup>b</sup>		0.84	82	8.48	26.2			24	185
SiO <sub>2</sub> -Fe-N-C	5.7 at 0.2 V	0.8							153
Fe-N-NG/RGO		0.84	63					5 <sup>m</sup>	146

TABLE II. (Continued.)

Catalyst	Kinetic current density $j_k$ (mA/cm <sup>2</sup> )	Half-wave potential $E_{1/2}$ (V)	Tafel slope $b$ (mV/dec)	Mass activity MA (mA/mg)	Specific activity SA (mA/cm <sup>2</sup> )	Electrochemical surface area ECSA (m <sup>2</sup> /g)	Retained current density after ADT (%)	Loss in $E_{1/2}$ after ADT (mV)	References
Fe–N–S–CNN <sup>b</sup>		0.78							151
(Fe,Ni)–N–C								12 <sup>c</sup>	179
(Fe,Ni)–N–C		0.84	60				92 <sup>a</sup>		164
Fe–O/C–N <sup>b</sup>	3.0 at 0.8 V	0.81						64	170
Mn–N–C <sup>b</sup>		0.78						20	133
NiN		0.49							123
Ti–MOF		0.75	18						134
Zn–N–C		0.75							135

<sup>a</sup>After 30000 s of chronoamperometry.

<sup>b</sup>In 0.5 M H<sub>2</sub>SO<sub>4</sub>

<sup>c</sup>After 10000 s of chronoamperometry.

<sup>d</sup>After 40000 s of chronoamperometry.

<sup>e</sup>After 5000 potential cycles of ADT.

<sup>f</sup>After 30000 potential cycles of ADT.

<sup>g</sup>After 50000 s of chronoamperometry.

<sup>h</sup>After 20000 potential cycles of ADT.

<sup>i</sup>After 20000 s of chronoamperometry.

<sup>j</sup>After 24 h of chronoamperometry.

<sup>k</sup>With respect to BET surface area.

<sup>l</sup>After 3000 potential cycles of ADT.

<sup>m</sup>After 15000 potential cycles of ADT.

Fe and N on RGO with minimal loss after 15000 potential cycles.<sup>146</sup>

Co–N–C catalysts have also been researched.<sup>152,161,176–178</sup> Although Co–N–C so far has shown lower catalytic activity than Fe–N–C (Table II), Co ions are less critical when released into both the membrane and ionomer since they are not Fenton active, and hence, a better durability is expected.<sup>161</sup> However, the Co–N–C needs advanced engineering to reach potentials comparable to Fe–N–C and Pt. Although half-wave potentials of up to 0.84 V vs RHE have been reached by a surfactant-covered Co–N–C structure,<sup>176</sup> they need to be further stabilized to achieve the superior durability expected.

Promising results have also been obtained by adding more than one metal to the M–N–C such as Fe–Ni,<sup>164,179</sup> Co–In,<sup>180</sup> Co–Ni,<sup>181</sup> and Co–Zn.<sup>150,182,183</sup> Zang *et al.* reported increased activity, both experimentally and from DFT calculations, due to Co–Ni dual active sites,<sup>182</sup> similar to the results produced by Ye and co-workers using Fe–Fe dual sites.<sup>184</sup> Fe–Fe was also studied by Zhang *et al.* by thermal migration of adjacent FeN<sub>4</sub> sites to form Fe<sub>2</sub>N<sub>6</sub> dual sites. These dual sites show high selectivity toward the four electron ORR due to the ability to adsorb two O atoms simultaneously.<sup>185</sup> On the other hand, Zhu *et al.* found that Fe and Ni formed single atom sites.<sup>164</sup> This shows the immense number of variations that can be found for SACs, while only a handful has yet been explored, and that further research is needed to find a durable catalyst with a high catalytic efficiency and low production cost.

## B. Durability issues

He *et al.* observed an initial high rate of degradation before an apparent stabilization of the Co–N–C. This is similar to what is found in PGM based catalysts and is due to an initial loss of unstable catalytic sites and oxidation of carbon.<sup>176</sup>

Kumar *et al.* found that carbon corrosion is occurring also in Fe–N–C catalysts. The deactivation of the catalyst is increased by the H<sub>2</sub>O<sub>2</sub> byproduct from the ORR on the Fe–N–C, as there is significant increase in corrosion when cycled in O<sub>2</sub> compared to Ar.<sup>144</sup> Bae *et al.* studied the effect of H<sub>2</sub>O<sub>2</sub> with varying pH. With the decrease in pH in the presence of H<sub>2</sub>O<sub>2</sub>, the amount of oxygen in the sample after the test increased. This is in accordance with the fact that Fenton's reaction is pH dependent and results in reducing the turnover frequency of nearby active sites.<sup>186</sup>

Doping graphene, CNTs, or CNWs with a transition metal and nitrogen has been proven by several groups to increase the durability,<sup>146,154,178</sup> with a further advantage of ensuring good conductivity in the catalyst layer.<sup>182</sup>

A major advantage of the SACs is that they are superior to Pt/C when it comes to methanol tolerance.<sup>148,151</sup> This would lower demands on gas purity for the PEMFC, which further reduces the operating costs.

## IV. PEM FUEL CELL TESTING

While the electrochemical activity of a catalyst can be tested in a three electrode setup, PEMFC testing is required to evaluate the

**TABLE III.** Characteristics of PEMFC tests in H<sub>2</sub>/O<sub>2</sub> for different electrocatalysts at 80 °C and 100% relative humidity. ADT refers to cycling between 0.6 V and 1.0 V unless stated otherwise.

Catalyst	Peak power density P <sub>max</sub> (W/cm <sup>2</sup> )	Cathode loading (mg/cm <sup>2</sup> )	Open circuit voltage OCV (V)	Specific activity SA (A/cm <sup>2</sup> )	Mass activity MA (A/g)	Tafel slope <i>b</i> (mV/dec)	Current retention after ADT (%)	Retention of ECSA after ADT (%)	References
C(N,S)	0.28	2.5	0.78						128
Co-N-C	0.87	4	0.92						176
Co-N-C	0.92	4							161
(Co,Zn)-N-CNW	0.60	4	0.88						182
Fe-N-C	1.18	2.7							142
Fe-N-C	0.48	4							139
Fe-N-C	0.78	1							130
Fe-N-C	0.63	4					49 <sup>a</sup>		140
Fe-N-C	0.68	3		0.29					157
Fe-N-C	0.73	3.5	0.98						158
Fe-N-C	0.75	2							172
Fe-N-C	0.7	4	1.01						143
Fe-N-C	0.86	4							169
Fe-N-C	0.65	4							165
Fe-N-C	0.6	4.0							160
Fe-N-S-C	0.53	4							149
Fe <sub>2</sub> N <sub>6</sub> -C	0.845	4	0.98						185
Fe-Fe <sub>3</sub> C/C	0.24	2	0.77						141
Fe-Fe <sub>3</sub> C/Fe-N-C	0.76	4							166
Fe-O/C-N	1.05	3.0			2 070				170
(Fe,Ni)-N-C	0.22	4							179
(Fe,Ni)-N-C	0.58	4	0.96						164
SiO <sub>2</sub> -Fe-N-C	0.32	3							153
(Zn,Co)-N-C	0.71								183
C(P,N)	0.14	3.5	0.86						127
Ir-N-C	0.93	4 (0.008 <sup>b</sup> )	0.955						100
Ir-N-C	0.87	3 (0.135 <sup>b</sup> )							102
Pt/C	1.39	0.11 <sup>c</sup>			400	90			94
Pt/C-N	0.33	0.5 <sup>c</sup>	0.93						120
Pt/Co-N/C	1.25	0.175 <sup>c</sup>							10
Pt/Nb-O/CNT	0.77	0.15					96 <sup>d</sup>		87
Pt/Ti-Nb-O		0.2						77 <sup>e</sup>	82
Pt/Ti(N,C)O	0.74						94 <sup>f</sup>		85
Pt-Co/C	1.16	0.1 <sup>c</sup>			720		61		15
Pt-Ni/C	1.21	0.1 <sup>c</sup>			660		65		15
Pt-Co/CNT/C	1.02	0.06 <sup>c</sup>							22
Pt-Cu/C		0.4	0.39						189
Pt-Cu-Ni/C	0.46	0.2 <sup>c</sup>							46
Pt-Fe/C		0.4	0.45						189
Pt-Fe/C	1.08	0.3							92
Pt-Fe/C	0.96	0.01 <sup>c</sup>			1 620		50 <sup>g</sup>		30
Pt-Ni/C		0.4	0.47						189
Pt-Ni/C	0.82	0.3							92
Pt-Ni/C	0.88	0.31		3.26	70	38	72 <sup>h</sup>	40 <sup>h</sup>	14
Pt-Ni-Mo/C	0.7 <sup>i</sup>	0.1 <sup>c</sup>			450 <sup>j</sup>				39
Pt-Pd/C	1.14	0.3							92
Pt-Pd/C-CNT	0.31 <sup>k</sup>	0.5 <sup>c</sup>					96 <sup>h</sup>		63



TABLE III. (Continued.)

Catalyst	Peak power density $P_{\max}$ (W/cm <sup>2</sup> )	Cathode loading (mg/cm <sup>2</sup> )	Open circuit voltage OCV (V)	Specific activity SA (A/cm <sup>2</sup> )	Mass activity MA (A/g)	Tafel slope $b$ (mV/dec)	Current retention after ADT (%)	Retention of ECSA after ADT (%)	References
Pt–Zn/C	2.00				520		83 <sup>g</sup>		38
Ru–N–C	0.64	4	0.93				76 <sup>l</sup>		101

<sup>a</sup>After 8 h at constant voltage.

<sup>b</sup>PGM loading.

<sup>c</sup>Pt loading.

<sup>d</sup>After 96 h at maximum current.

<sup>e</sup>After 500 potential cycles from 1.0 V to 1.5 V.

<sup>f</sup>After 5000 potential cycles from 1.0 V to 1.5 V.

<sup>g</sup>After 30000 potential cycles of ADT.

<sup>h</sup>After 3000 potential cycles of ADT.

<sup>i</sup>Value determined under H<sub>2</sub>/air supply.

<sup>j</sup>With respect to Pt mass.

<sup>k</sup>At 60 °C.

<sup>l</sup>After 100 h of constant operation.

performance of the catalyst when the electrolyte is changed from liquid to solid. However, comparison of the catalyst performance in a PEMFC is more complex. In Tables III and IV, test conditions and reported performance are shown for PEMFC tests using H<sub>2</sub>/O<sub>2</sub> and H<sub>2</sub>/air, respectively. Many parameters of PEMFC testing affect the results, although they are reported in varying degrees. The ionomer content in the catalyst layer and coating technique on membrane affect the proton conduction from the catalyst layer. The type of support, choice of gas diffusion layer (GDL), and compression of the cell affect the electrical conductivity. Finally, the porosity in GDL and catalyst layer and the flow field design and size of the cell affect how homogeneously the reactant gases are distributed across the catalyst layer.

Half of the reported tests use air at the cathode, while the rest use O<sub>2</sub>. Several groups, testing both PGM and PGM-free catalysts, have tested their catalyst in both and found that the peak power density is almost twice as high when using O<sub>2</sub> compared to air.<sup>22,130,169,172</sup> Using pure oxygen mitigates some of the mass transport limitations and is more comparable to using air. Contaminants in air are rarely specified, but it is known that CO and SO<sub>2</sub> both poison the catalyst.<sup>187,188</sup>

For PGM containing catalysts, the catalyst layer has a thickness of 10 μm and the catalyst loading varies between 0.06 and 0.4 mg/cm<sup>2</sup>. The focus of the current research is on improving the corrosion resistance of the carbon support.<sup>92–95</sup> Daş *et al.* tested Pt–M alloys as the anode, cathode, and both and found that the highest performance gain was obtained when the bimetallic catalysts were applied as the anode.<sup>189</sup>

A highly desirable durability in PEMFC application was achieved by Gao *et al.*, where the performance did not decrease even after 50 000 potential cycles of ADT for a Pt–Co/CNW catalyst (Fig. 14).<sup>9</sup>

For PGM-free catalysts, low volumetric activity leads to ten times thicker catalyst layers. Consequently, mass transport and resistance problems that are minimized or already overcome for noble

metal catalyst needs to be solved. It should also be noted that although 4 mg/cm<sup>2</sup> is a common loading for SACs, some of the best performances come from catalysts with half the loading.<sup>142</sup> In a recent review by Satjaritanun and Zenyuk, pooling of water at interfaces between the catalyst layer and the microporous layer or the membrane as a result of non-homogeneous fabrication was found as an obstacle for these catalysts.<sup>190</sup> Liu *et al.* concluded that the hydrophobicity of the catalyst layer was the reason for water accumulation in a study where both the catalyst coated membrane and gas diffusion electrode assemblies were analyzed.<sup>191</sup> Yang *et al.* kept the SiO<sub>2</sub> support in the Fe–N–C catalyst, which increased the hydrophobicity of the catalyst layer and thus improved the PEMFC performance.<sup>153</sup>

Furthermore, it was concluded that although flooding of micropores is often cited as a major degradation mechanism and it can block O<sub>2</sub> transport to the active site, it is not the most important. In the review by Satjaritanun and Zenyuk, Fe–N<sub>4</sub> demetalization was instead pointed out as the major degradation mechanism.<sup>190</sup> Electrochemical impedance spectroscopy of aged PEMFCs with Fe–N–C catalysts has confirmed that there is a loss of active sites, which further leads to Fe-ion poisoning of the ionomer and membrane.<sup>192,193</sup>

It should be noted that in alkaline environment, many of the PGM-free catalysts have higher performance than the Pt-based catalyst. Therefore, these catalysts would have an advantage if the PEM was changed to an anion exchange membrane (AEM), ensuring a less corrosive environment in the cell. Seeberger *et al.* demonstrated the feasibility of a bipolar membrane assembly for PGM-free FCs, combining the alkaline ORR with acidic hydrogen oxidation reaction (HOR) by joining a PEM with an AEM as a double membrane.<sup>194</sup>

Fe–N–C has also been pointed out to be an alternative to Pt/C in high temperature PEMFCs. In these cases, where the membrane is polybenzimidazol doped with phosphoric acid, Pt is poisoned by the phosphate ions, while Fe–N–C is immune to the poisoning effect.<sup>156</sup>

**TABLE IV.** Characteristics of PEMFC tests in H<sub>2</sub>/air for different electrocatalysts at 80 °C and 100% relative humidity. ADT refers to cycling between 0.6 V and 1.0 V unless stated otherwise.

Catalyst	Peak power density P <sub>max</sub> (W/cm <sup>2</sup> )	Cathode loading (mg/cm <sup>2</sup> )	Open circuit voltage OCV (V)	Specific activity SA (A/cm <sup>2</sup> )	Mass activity MA (A/g)	Tafel slope b (mV/dec)	Current retention after ADT (%)	Retention of ECSA after ADT (%)	References
Fe-N-C	0.42	2							142
Fe-N-C	0.46	1					68 <sup>a</sup>		130
Fe-N-C	0.35	2							172
Fe-N-C	0.43	4							169
Pt/C		0.22			800				115
Pt/C <sup>b</sup>	0.78	0.10		1.15			91 <sup>c</sup>	67	188
Pt/C	0.85	0.1							81
Pt/C	1.20	0.07							96
Pt(N)/C	1.25	0.3							54
Pt/Nb-O/C		0.10			288		68 <sup>c</sup>		83
Pt/Ti-C-O/CNT	0.18 <sup>b</sup>	0.2							80
Pt-Co/CNW	0.71	0.09 <sup>d</sup>					107 <sup>e</sup>		9
Pt-Ni/C <sup>f</sup>	0.88	0.4 <sup>d</sup>					88 <sup>g</sup>		16
Pt-Ni/C	0.92	0.15					>97 <sup>h</sup>		12
Pt-Ni-Ir/C	0.40	0.35 <sup>d</sup>					80 <sup>i</sup>		45
Pt/C + Pd-Au <sup>j</sup>	0.54 <sup>b</sup>	0.1 <sup>d</sup>			160		79 <sup>k</sup>	68 <sup>c</sup>	56
Pt/Mn/C		0.12			373			66 <sup>l</sup>	93
Pt-Co/C		0.11 <sup>d</sup>		0.002	560	63	81 <sup>c</sup>		8
Pt <sub>3</sub> Co/C			0.98				85 <sup>m</sup>	79 <sup>n</sup>	98
Pt-Co/CNT/C	0.54	0.06 <sup>d</sup>							22
Pt-Ir/C		0.4 <sup>d</sup>					99 <sup>k</sup>		34
Pt-Y-O/C	0.84	0.4							51

<sup>a</sup>Voltage retention after 10 h at constant-current operation.<sup>b</sup>Tests performed at 60 °C.<sup>c</sup>After 30000 potential cycles of ADT.<sup>d</sup>Pt loading<sup>e</sup>After 50000 potential cycles of ADT.<sup>f</sup>Tests performed at 80% relative humidity<sup>g</sup>After 100 h at constant voltage.<sup>h</sup>After 180 h at constant voltage.<sup>i</sup>After 1000 potential cycles of ADT.<sup>j</sup>Pd-Au NPs are coated onto the Nafion membrane, while a conventional Pt/C catalyst is used in addition.<sup>k</sup>After 15000 potential cycles of ADT.<sup>l</sup>After 5000 potential cycles from 1.0 to 1.5 V.<sup>m</sup>After 20000 potential cycles of ADT.<sup>n</sup>After 10000 potential cycles of ADT.

## V. RECYCLING OF PEMFC

Recycling of PEMFC components and particularly of PGM electrocatalysts is of utmost importance considering the current striving toward sustainability. Yet, this is an aspect that deserves larger attention from the scientific community in the field.

Lotrič *et al.* performed a life cycle assessment of the PEMFC stack and found that Pt is the component in the PEMFC with the largest environmental impact, and hence, recycling of the Pt can reduce the environmental footprint of the PEMFC.<sup>195</sup> In general, the global recycling of PGM has the potential to over 95% recovery.<sup>196</sup> For PGM used in PEMFC specifically, Sharma *et al.* have

shown that Pt can be dissolved from a gas diffusion electrode by electrochemical dissolution in HCl, with a recovery efficiency of more than 90% when producing a new catalyst from the recycled material.<sup>197,198</sup> However, the gas diffusion electrode was never assembled or cycled before dissolution, and the recovery efficiency may therefore be lower considering Pt dissolution and migration into the membrane and the fact that Pt particles adhered to the membrane upon disassembly. Duclos *et al.* studied the recovery of PtCo from an MEA by two different hydrometallurgical routes. Both methods include incineration of fluorinated polymers, causing emissions, and the authors point out the need for recycling of the fluorinated polymers as well. The ion exchange resin and solvent separation methods

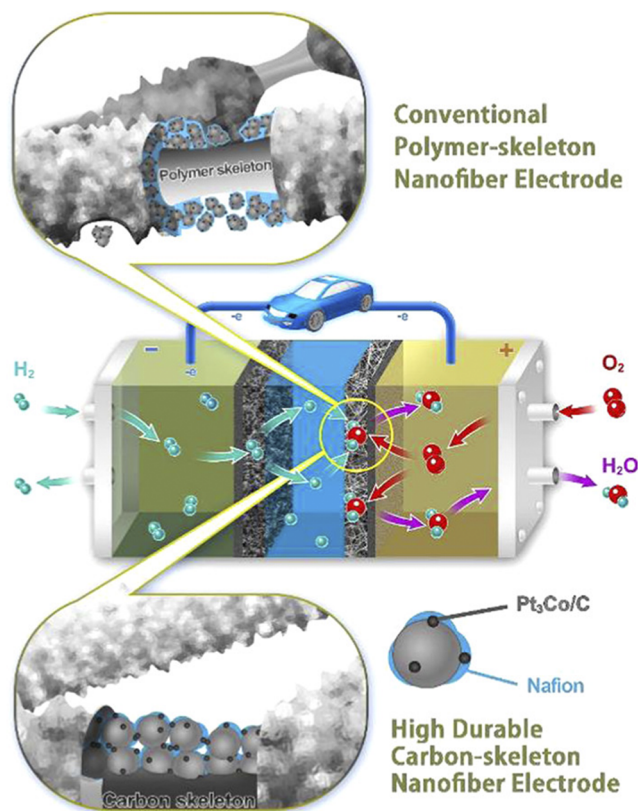


**FIG. 14.** Illustration of the CNW-supported Pt-Co catalyst in the PEMFC setup, which reached 8.2 W/mg<sub>Pt</sub>.<sup>9</sup> Reprinted with permission from Gao *et al.*, *ACS Sustainable Chem. Eng.* **8**, 13030 (2020). Copyright 2020 American Chemical Society.

gave Pt yield of 77% and 83%, respectively, while the ion exchange resin is advantageous with respect to synthesizing a new catalyst material from the product.<sup>4</sup>

## VI. SUMMARY

Pt remains as the most important component of reliable and efficient PEMFC ORR electrocatalysts—and will continue to do so for the time being. The cost of the fuel cell stacks can be efficiently reduced by lowering the amount of Pt used and by increasing its efficiency through alloying, shape-tuning, and creating NPs with Pt-rich surfaces.

Among the most recent studies, the most promising way for maximizing the efficiency and durability lies in the combination of different approaches: the alloying of Pt with a transition metal, the synthesis of hollow NPs, and the fixation of NPs in an enclosing carbon-based structure, which can prevent the most prominent durability issues, namely, the growth of Pt NPs, and the leaching of Pt alloys. With further reduction of the amount of Pt used and recycling of the MEA after utilization, the impact of the Pt in the PEMFC can be reduced to levels comparable to that from PGMs used in the catalysts of internal combustion engines.

Another important durability issue occurring at high potential cycling, the corrosion of the carbon support, can be tackled by replacing or modifying the carbon support material. Many different approaches and materials have been studied to modify the support of PGM-based catalysts, showing desirable improvements. Considering the high amount of studies on the field in general, optimized support structures can soon be combined with optimized PGM catalysts in order to eliminate all durability issues and to provide reliable performance at low Pt loading. As there is a well-established industry for the production of carbon supported Pt NPs, these improvements can be implemented without needing major changes, and so, the way to commercialization is relatively short.

Regarding PGM-free catalysts, sufficient durability is the key issue. As a result of this being a new technology, current work focuses on performance optimization, while works focusing on their durability are rather scarce. For the SACs, solutions have to be found to effectively prevent metal dissolution in acidic environments and increase durability during potential cycling. Furthermore, optimization of the catalyst layer in the PEMFC, achieving a more homogeneous deposition, and upscaling of the fabrication are key to bringing these catalysts closer to broad commercialization. Otherwise, SACs are readily applicable in AEMFCs.

## AUTHORS' CONTRIBUTIONS

L.M. and K.E. contributed equally to this work.

## ACKNOWLEDGMENTS

This work received funding from the European Union's Horizon 2020 research and innovation programme under the Marie Skłodowska-Curie Grant Agreement No. 764977. E.P. also acknowledges funding from the Generalitat de Catalunya under Project No. 2017-SGR-292.

## DATA AVAILABILITY

Data sharing is not applicable to this article as no new data were created or analyzed in this study.

## REFERENCES

- <sup>1</sup>B. G. Pollet, S. S. Kocha, and I. Staffell, "Current status of automotive fuel cells for sustainable transport," *Curr. Opin. Electrochem.* **16**, 90 (2019).
- <sup>2</sup>Fuel Cell Technologies Office, "DOE technical targets for polymer electrolyte membrane fuel cell components," in *Multi-Year Research, Development, and Demonstration Plan (2017)*, Chap. 3.4 Fuel Cells.
- <sup>3</sup>M. Shao, Q. Chang, J.-P. Dodelet, and R. Chenitz, "Recent advances in electrocatalysts for oxygen reduction reaction," *Chem. Rev.* **116**, 3594 (2016).
- <sup>4</sup>L. Duclos, R. Chattot, L. Dubau, P.-X. Thivel, G. Mandil, V. Laforest, M. Bolloli, R. Vincent, and L. Svecova, "Closing the loop: Life cycle assessment and optimization of a PEMFC platinum-based catalyst recycling process," *Green Chem.* **22**, 1919 (2020).
- <sup>5</sup>Q. Deng, J. Han, J. Zhao, G. Chen, T. Vegge, and H. A. Hansen, "1D metal-dithiolene wires as a new class of bi-functional oxygen reduction and evolution single-atom electrocatalysts," *J. Catal.* **393**, 140 (2021).

- <sup>6</sup>A. Jain, Z. Wang, and J. K. Nørskov, "Stable two-dimensional materials for oxygen reduction and oxygen evolution reactions," *ACS Energy Lett.* **4**, 1410 (2019).
- <sup>7</sup>T. Yoshida and K. Kojima, "Toyota MIRAI fuel cell vehicle and progress toward a future hydrogen society," *Interface* **24**, 45 (2015).
- <sup>8</sup>J. Li, S. Sharma, X. Liu, Y.-T. Pan, J. S. Spendelow, M. Chi, Y. Jia, P. Zhang, D. A. Cullen, Z. Xi *et al.*, "Hard-magnet L<sub>10</sub>-CoPt nanoparticles advance fuel cell catalysis," *Joule* **3**, 124 (2019).
- <sup>9</sup>Y. Gao, M. Hou, L. He, M. Qi, H. Chen, W. Luo, and Z. Shao, "Performance- and durability-enhanced carbon-skeleton nanofiber electrode with Pt<sub>3</sub>Co/C for PEMFCs," *ACS Sustainable Chem. Eng.* **8**, 13030 (2020).
- <sup>10</sup>B. Hu, X. Deng, L. Zhou, J. Dai, G. Yang, W. Tan, W. Zhou, and Z. Shao, "Facile synthesis of synergistic Pt/(Co-N)@C composites as alternative oxygen-reduction electrode of PEMFCs with attractive activity and durability," *Compos., Part B* **193**, 108012 (2020).
- <sup>11</sup>J. Sriwannaboot, A. Kannan, and N. Tantavichet, "Pulse-reverse electrodeposition of Pt-Co bimetallic catalysts for oxygen reduction reaction in acidic medium," *Int. J. Hydrogen Energy* **45**, 7025 (2020).
- <sup>12</sup>X. Tian, X. Zhao, Y.-Q. Su, L. Wang, H. Wang, D. Dang, B. Chi, H. Liu, E. J. M. Hensen, X. W. Lou, and B. Y. Xia, "Engineering bunched Pt-Ni alloy nanocages for efficient oxygen reduction in practical fuel cells," *Science* **366**, 850 (2019).
- <sup>13</sup>Q. Zhao, C. Wang, H. Wang, J. Wang, Y. Tang, Z. Mao, and K. Sasaki, "H<sub>2</sub>-induced thermal treatment significantly influences the development of a high performance low-platinum core-shell PtNi/C alloyed oxygen reduction catalyst," *Int. J. Energy Res.* **44**, 4773 (2020).
- <sup>14</sup>P. Mardle, G. Thirunavukkarasu, S. Guan, Y.-L. Chiu, and S. Du, "Comparative study of PtNi nanowire array electrodes toward oxygen reduction reaction by half-cell measurement and PEMFC test," *ACS Appl. Mater. Interfaces* **12**, 42832 (2020).
- <sup>15</sup>Z. Zhao, M. D. Hossain, C. Xu, Z. Lu, Y.-S. Liu, S.-H. Hsieh, I. Lee, W. Gao, J. Yang, B. V. Merinov, W. Xue, Z. Liu, J. Zhou, Z. Luo, X. Pan, F. Zaera, J. Guo, X. Duan, W. A. Goddard III, and Y. Huang, "Tailoring a three-phase microenvironment for high-performance oxygen reduction reaction in proton exchange membrane fuel cells," *Matter* **3**, 1774 (2020).
- <sup>16</sup>B. Li, J. Wang, X. Gao, C. Qin, D. Yang, H. Lv, Q. Xiao, and C. Zhang, "High performance octahedral PtNi/C catalysts investigated from rotating disk electrode to membrane electrode assembly," *Nano Res.* **12**, 281 (2019).
- <sup>17</sup>Z. Jiang, Y. Liu, L. Huang, W. H. Gong, and P. K. Shen, "A facile method to synthesize Pt-Ni octahedral nanoparticles with porous and open structure features for enhanced oxygen reduction catalysis," *ACS Sustainable Chem. Eng.* **7**, 8109 (2019).
- <sup>18</sup>F. Kong, Z. Ren, M. N. Banis, L. Du, X. Zhou, G. Chen, L. Zhang, J. Li, S. Wang, M. Li, K. Doyle-Davis, Y. Ma, R. Li, A. Young, L. Yang, M. Markiewicz, Y. Tong, G. Yin, C. Du, J. Luo, and X. Sun, "Active and stable Pt-Ni alloy octahedra catalyst for oxygen reduction via near-surface atomic engineering," *ACS Catal.* **10**, 4205 (2020).
- <sup>19</sup>S. Kühn, M. Gocyla, H. Heyen, S. Selve, M. Heggen, R. E. Dunin-Borkowski, and P. Strasser, "Concave curvature facets benefit oxygen electroreduction catalysis on octahedral shaped PtNi nanocatalysts," *J. Mater. Chem. A* **7**, 1149 (2019).
- <sup>20</sup>J. Wang, X. Zhou, B. Li, D. Yang, H. Lu, Q. Xiao, P. Ming, X. Wei, and C. Zhang, "Highly efficient, cell reversal resistant PEMFC based on PtNi/C octahedral and OER composite catalyst," *Int. J. Hydrogen Energy* **45**, 8930 (2020).
- <sup>21</sup>W. Gong, Z. Jiang, R. Wu, Y. Liu, L. Huang, N. Hu, P. Tsiakaras, and P. K. Shen, "Cross-double dumbbell-like Pt-Ni nanostructures with enhanced catalytic performance toward the reactions of oxygen reduction and methanol oxidation," *Appl. Catal. B* **246**, 277 (2019).
- <sup>22</sup>J. Wang, G. Wu, W. Wang, W. Xuan, J. Jiang, J. Wang, L. Li, W.-F. Lin, W. Ding, and Z. Wei, "A neural-network-like catalyst structure for the oxygen reduction reaction: Carbon nanotube bridged hollow PtCo alloy nanoparticles in a MOF-like matrix for energy technologies," *J. Mater. Chem. A* **7**, 19786 (2019).
- <sup>23</sup>Q. Zhao, C. Wang, H. Wang, J. Wang, Y. Tang, Z. Mao, and K. Sasaki, "Synthesis of a high-performance low-platinum PtAg/C alloyed oxygen reduction catalyst through the gradual reduction method," *New J. Chem.* **44**, 3728 (2020).
- <sup>24</sup>Y. Feng, Q. Shao, F. Lv, L. Bu, J. Guo, S. Guo, and X. Huang, "Intermetallic PtBi nanoplates boost oxygen reduction catalysis with superior tolerance over chemical fuels," *Adv. Sci.* **7**, 1800178 (2020).
- <sup>25</sup>M. Gatalo, F. Ruiz-Zepeda, N. Hodnik, G. Dražič, M. Bele, and M. Gaberšček, "Insights into thermal annealing of highly-active PtCu<sub>3</sub>/C oxygen reduction reaction electrocatalyst: An in-situ heating transmission electron microscopy study," *Nano Energy* **63**, 103892 (2019).
- <sup>26</sup>L. Zhang, X.-F. Zhang, X.-L. Chen, A.-J. Wang, D.-M. Han, Z.-G. Wang, and J.-J. Feng, "Facile solvothermal synthesis of Pt<sub>71</sub>Co<sub>29</sub> lamellar nanoflowers as an efficient catalyst for oxygen reduction and methanol oxidation reactions," *J. Colloid Interface Sci.* **536**, 556 (2019).
- <sup>27</sup>Z. Yang, L. Shang, X. Xiong, R. Shi, G. I. N. Waterhouse, and T. Zhang, "Hollow PtFe alloy nanoparticles derived from Pt-Fe<sub>3</sub>O<sub>4</sub> dimers through a silica-protection reduction strategy as efficient oxygen reduction electrocatalysts," *Chem. Eur. J.* **26**, 4090 (2020).
- <sup>28</sup>M. Gong, J. Zhu, M. Liu, P. Liu, Z. Deng, T. Shen, T. Zhao, R. Lin, Y. Lu, S. Yang, Z. Liang, S. M. Bak, E. Stavitski, Q. Wu, R. R. Adzic, H. L. Xin, and D. Wang, "Optimizing PtFe intermetallics for oxygen reduction reaction: From DFT screening to in situ XAFS characterization," *Nanoscale* **11**, 20301 (2019).
- <sup>29</sup>Z. Meng, F. Xiao, Z. Wei, X. Guo, Y. Zhu, Y. Liu, G. Li, Z.-Q. Yu, M. Shao, and W.-Y. Wong, "Direct synthesis of L<sub>10</sub>-FePt nanoparticles from single-source bimetallic complex and their electrocatalytic applications in oxygen reduction and hydrogen evolution reactions," *Nano Res.* **12**, 2954 (2019).
- <sup>30</sup>J. Choi, Y. J. Lee, D. Park, H. Jeong, S. Shin, H. Yun, J. Lim, J. Han, E. J. Kim, S. S. Jeon, Y. Jung, H. Lee, and B. J. Kim, "Highly durable fuel cell catalysts using crosslinkable block copolymer-based carbon supports with ultralow Pt loadings," *Energy Environ. Sci.* **13**, 4921 (2020).
- <sup>31</sup>J. Zhu, A. O. Elnabawy, Z. Lyu, M. Xie, E. A. Murray, Z. Chen, W. Jin, M. Mavrikakis, and Y. Xia, "Facet-controlled Pt-Ir nanocrystals with substantially enhanced activity and durability towards oxygen reduction," *Mater. Today* **35**, 69 (2020).
- <sup>32</sup>J.-Y. Park, H.-S. Park, S.-B. Han, D.-H. Kwak, J.-E. Won, T. Lim, and K.-W. Park, "Organic ligand-free PtIr alloy nanostructures for superior oxygen reduction and evolution reactions," *J. Ind. Eng. Chem.* **77**, 105 (2019).
- <sup>33</sup>D. Fang, X. Tang, L. Yang, D. Xu, H. Zhang, S. Sun, Z. Shao, and B. Yi, "Facile synthesis of Pt-decorated Ir black as a bifunctional oxygen catalyst for oxygen reduction and evolution reactions," *Nanoscale* **11**, 9091 (2019).
- <sup>34</sup>J. Bak, H. Kim, S. Lee, M. Kim, E.-J. Kim, J. Roh, J. Shin, C. H. Choi, and E. Cho, "Boosting the role of Ir in mitigating corrosion of carbon support by alloying with Pt," *ACS Catal.* **10**, 12300 (2020).
- <sup>35</sup>A. Brouzgou, A. Seretis, S. Song, P. K. Shen, and P. Tsiakaras, "CO tolerance and durability study of PtMe (Me = Ir or Pd) electrocatalysts for H<sub>2</sub>-PEMFC application," *Int. J. Hydrogen Energy* (published online, 2020).
- <sup>36</sup>H. Gao, S. Liao, Y. Zhang, X. Jia, L. Zhou, Z. Zheng, and Y. Yang, "Methanol-tolerant SePt/C: Effects of Se content on the structure and electrocatalytic performance for oxygen reduction reaction," *Ionics* **26**, 1315 (2020).
- <sup>37</sup>H. Wang, S. Yin, C. Li, K. Deng, Z. Wang, Y. Xu, X. Li, H. Xue, and L. Wang, "Direct synthesis of superlong Pt-Te mesoporous nanotubes for electrocatalytic oxygen reduction," *J. Mater. Chem. A* **7**, 1711 (2019).
- <sup>38</sup>J. Liang, Z. Zhao, N. Li, X. Wang, S. Li, X. Liu, T. Wang, G. Lu, D. Wang, B. J. Hwang, Y. Huang, D. Su, and Q. Li, "Biaxial strains mediated oxygen reduction electrocatalysis on Fenton reaction resistant L<sub>10</sub>-PtZn fuel cell cathode," *Adv. Energy Mater.* **10**, 2000179 (2020).
- <sup>39</sup>F. Dionigi, C. C. Weber, M. Primbs, M. Gocyla, A. Martinez Bonastre, C. Spöri, H. Schmies, E. Hornberger, S. Kühn, J. Drnec, M. Heggen, J. Sharman, R. E. Dunin-Borkowski, and P. Strasser, "Controlling near-surface Ni composition in octahedral PtNi(Mo) nanoparticles by Mo doping for a highly active oxygen reduction reaction catalyst," *Nano Lett.* **19**, 6876 (2019).
- <sup>40</sup>L. Cao, Z. Zhao, Z. Liu, W. Gao, S. Dai, J. Gha, W. Xue, H. Sun, X. Duan, X. Pan, T. Mueller, and Y. Huang, "Differential surface elemental distribution leads to significantly enhanced stability of PtNi-based ORR catalysts," *Matter* **1**, 1567 (2019).
- <sup>41</sup>X. Shen, S. Dai, Y. Pan, L. Yao, J. Yang, X. Pan, J. Zeng, and Z. Peng, "Tuning electronic structure and lattice diffusion barrier of ternary Pt-In-Ni for both

- improved activity and stability properties in oxygen reduction electrocatalysis," *ACS Catal.* **9**, 11431 (2019).
- <sup>42</sup>W. Tu, W. Luo, C. Chen, K. Chen, E. Zhu, Z. Zhao, Z. Wang, T. Hu, H. Zai, X. Ke, M. Sui, P. Chen, Q. Zhang, Q. Chen, Y. Li, and Y. Huang, "Tungsten as 'adhesive' in Pt<sub>2</sub>CuW<sub>0.25</sub> ternary alloy for highly durable oxygen reduction electrocatalysis," *Adv. Funct. Mater.* **30**, 1908230 (2020).
- <sup>43</sup>Z. Wang, X. Yao, Y. Kang, D. Xia, and L. Gan, "Rational development of structurally ordered platinum ternary intermetallic electrocatalysts for oxygen reduction reaction," *Catalysts* **9**, 569 (2019).
- <sup>44</sup>R. Sriphathoorat, K. Wang, and P. K. Shen, "Trimetallic hollow Pt–Ni–Co nanodendrites as efficient anodic electrocatalysts," *ACS Appl. Energy Mater.* **2**, 961 (2019).
- <sup>45</sup>R. Lin, L. Che, D. Shen, and X. Cai, "High durability of Pt–Ni–Ir/C ternary catalyst of PEMFC by stepwise reduction synthesis," *Electrochim. Acta* **330**, 135251 (2020).
- <sup>46</sup>X. Wang, L. Zhang, F. Wang, J. Yu, and H. Zhu, "Nickel-introduced structurally ordered PtCuNi/C as high performance electrocatalyst for oxygen reduction reaction," *Prog. Nat. Sci.* **30**, 905 (2020).
- <sup>47</sup>C. He, Z. Ma, Q. Wu, Y. Cai, Y. Huang, K. Liu, Y. Fan, H. Wang, Q. Li, J. Qi, Q. Li, and X. Wu, "Promoting the ORR catalysis of Pt–Fe intermetallic catalysts by increasing atomic utilization and electronic regulation," *Electrochim. Acta* **330**, 135119 (2020).
- <sup>48</sup>H. Chen, T. Zheng, Q. He, L. Shang, G. Wang, Q. Wang, X. Wang, X. Shi, M. Gu, and Z. Jiang, "Local coordination and ordering engineering to design efficient core-shell oxygen reduction catalysts," *J. Electrochem. Soc.* **167**, 144501 (2020).
- <sup>49</sup>L. Huang, M. Wei, N. Hu, P. Tsiakaras, and P. K. Shen, "Molybdenum-modified and vertex-reinforced quaternary hexapod nanoskeletons as efficient electrocatalysts for methanol oxidation and oxygen reduction reaction," *Appl. Catal. B* **258**, 117974 (2019).
- <sup>50</sup>W. Tu, K. Chen, L. Zhu, H. Zai, E. Bin, X. Ke, C. Chen, M. Sui, Q. Chen, and Y. Li, "Tungsten-doping-induced surface reconstruction of porous ternary Pt-based alloy electrocatalyst for oxygen reduction," *Adv. Funct. Mater.* **29**, 1807070 (2019).
- <sup>51</sup>T. Chu, M. Xie, D. Yang, P. Ming, B. Li, and C. Zhang, "Highly active and durable carbon support Pt-rare earth catalyst for proton exchange membrane fuel cell," *Int. J. Hydrogen Energy* **45**, 27291 (2020).
- <sup>52</sup>R. Guo, W. Bi, K. Zhang, Y. Liu, C. Wang, Y. Zheng, and M. Jin, "Phosphorization treatment improves the catalytic activity and durability of platinum catalysts toward oxygen reduction reaction," *Chem. Mater.* **31**, 8205 (2019).
- <sup>53</sup>Z. Pu, R. Cheng, J. Zhao, Z. Hu, C. Li, W. Li, P. Wang, I. S. Amiin, Z. Wang, M. Wang, D. Chen, and S. Mu, "Anion-modulated platinum for high-performance multifunctional electrocatalysis toward HER, HOR, and ORR," *iScience* **23**, 101793 (2020).
- <sup>54</sup>Y. Xiong, Y. Ma, L. Zou, S. Han, H. Chen, S. Wang, M. Gu, Y. Shen, L. Zhang, Z. Xia, J. Li, and H. Yang, "N-doping induced tensile-strained Pt nanoparticles ensuring an excellent durability of the oxygen reduction reaction," *J. Catal.* **382**, 247 (2020).
- <sup>55</sup>M. Luo, Z. Zhao, Y. Zhang, Y. Sun, Y. Xing, F. Lv, Y. Yang, X. Zhang, S. Hwang, Y. Qin, J.-Y. Ma, F. Lin, D. Su, G. Lu, and S. Guo, "PdMo bimetallic for oxygen reduction catalysis," *Nature* **574**, 81 (2019).
- <sup>56</sup>L. Wang, Y. Zhou, J. Timoshenko, S. Liu, Q. Qiao, K. Kisslinger, M. Ciuffo, Y.-C. Chuang, X. Zuo, Y. Xue, Y. Guo, C. Pan, H. Li, C.-Y. Nam, S. Bliznakov, P. Liu, A. I. Frenkel, Y. Zhu, and M. H. Rafailovich, "Designing nanoplatelet alloy/Nafion catalytic interface for optimization of PEMFCs: Performance, durability, and CO resistance," *ACS Catal.* **9**, 1446 (2019).
- <sup>57</sup>J. Uribe-Godínez and A. Altamirano-Gutiérrez, "Systematic study of iridium-based catalysts derived from Ir<sub>4</sub>(CO)<sub>12</sub>, capable to perform the ORR and HOR," *Catal. Today* (published online, 2020).
- <sup>58</sup>F. Chang, Z. Bai, M. Li, M. Ren, T. Liu, L. Yang, C.-J. Zhong, and J. Lu, "Strain-modulated platinum-palladium nanowires for oxygen reduction reaction," *Nano Lett.* **20**, 2416 (2020).
- <sup>59</sup>X. Deng, S. Yin, X. Wu, M. Sun, Z. Li, Z. Xie, Y. Liang, and Q. Huang, "Scalable preparation of PtPd/carbon nanowires in the form of membrane as highly stable electrocatalysts for oxygen reduction reaction," *Int. J. Hydrogen Energy* **44**, 2752 (2019).
- <sup>60</sup>R. Wu, Y. Li, W. Gong, and P. K. Shen, "One-pot synthesis of Pt–Pd bimetallic nanodendrites with enhanced electrocatalytic activity for oxygen reduction reaction," *ACS Sustainable Chem. Eng.* **7**, 8419 (2019).
- <sup>61</sup>R. Wu, P. Tsiakaras, and P. K. Shen, "Facile synthesis of bimetallic Pt–Pd symmetry-broken concave nanocubes and their enhanced activity toward oxygen reduction reaction," *Appl. Catal. B* **251**, 49 (2019).
- <sup>62</sup>M. Zhou, H. Wang, A. O. Elnabawy, Z. D. Hood, M. Chi, P. Xiao, Y. Zhang, M. Mavrikakis, and Y. Xia, "Facile one-pot synthesis of Pd@Pt<sub>111</sub> octahedra with enhanced activity and durability toward oxygen reduction," *Chem. Mater.* **31**, 1370 (2019).
- <sup>63</sup>Y. Y. Rivera-Lugo, K. I. Pérez-Muñoz, B. Trujillo-Navarrete, C. Silva-Carrillo, E. A. Reynoso-Soto, J. C. Calva Yañez, S. W. Lin, J. R. Flores-Hernández, and R. M. Félix-Navarro, "PtPd hybrid composite catalysts as cathodes for proton exchange membrane fuel cells," *Energies* **13**, 316 (2020).
- <sup>64</sup>H. Chen, R. Wu, and P. K. Shen, "One-pot fabrication of site-selective hexapod PtPdCu concave rhombic dodecahedrons as highly efficient catalysts for electrocatalysis," *ACS Sustainable Chem. Eng.* **8**, 1520 (2020).
- <sup>65</sup>Y. Deng, S. Yin, Y. Liu, Y. Lu, X. Cao, L. Wang, H. Wang, Y. Zhao, and H. Gu, "Mesoporous AgPdPt nanotubes as electrocatalysts for the oxygen reduction reaction," *ACS Appl. Nano Mater.* **2**, 1876 (2019).
- <sup>66</sup>F. Kong, S. Liu, J. Li, L. Du, M. N. Banis, L. Zhang, G. Chen, K. Doyle-Davis, J. Liang, S. Wang, F. Zhao, R. Li, C. Du, G. Yin, Z. Zhao, and X. Sun, "Trimetallic Pt–Pd–Ni octahedral nanocages with subnanometer thick-wall towards high oxygen reduction reaction," *Nano Energy* **64**, 103890 (2019).
- <sup>67</sup>C. Li, Y. Xu, K. Deng, S. Yin, Z. Wang, H. Xue, X. Li, L. Wang, and H. Wang, "Metal-nonmetal nanoarchitectures: Quaternary PtPdNiP mesoporous nanospheres for enhanced oxygen reduction electrocatalysis," *J. Mater. Chem. A* **7**, 3910 (2019).
- <sup>68</sup>H. Nan, Y.-Q. Su, C. Tang, R. Cao, D. Li, J. Yu, Q. Liu, Y. Deng, and X. Tian, "Engineering the electronic and strained interface for high activity of PdM<sub>core</sub>@Pt<sub>monolayer</sub> electrocatalysts for oxygen reduction reaction," *Sci. Bull.* **65**, 1396 (2020).
- <sup>69</sup>H. Wang, Y. Li, K. Deng, C. Li, H. Xue, Z. Wang, X. Li, Y. Xu, and L. Wang, "Trimetallic PtPdNi-truncated octahedral nanocages with a well-defined mesoporous surface for enhanced oxygen reduction electrocatalysis," *ACS Appl. Mater. Interfaces* **11**, 4252 (2019).
- <sup>70</sup>K. Deng, Y. Xu, Z. Dai, H. Yu, S. Yin, Z. Wang, X. Li, L. Wang, and H. Wang, "Enhanced oxygen reduction and methanol oxidation electrocatalysis over bifunctional PtPdIr mesoporous hollow nanospheres," *Chem.-Asian J.* **14**, 3868 (2019).
- <sup>71</sup>C. M. Sánchez-Sánchez, J. Solla-Gullón, F. J. Vidal-Iglesias, A. Aldaz, V. Montiel, and E. Herrero, "Imaging structure sensitive catalysis on different shape-controlled platinum nanoparticles," *J. Am. Chem. Soc.* **132**, 5622 (2010).
- <sup>72</sup>J.-C. Dong, X.-G. Zhang, V. Briega-Martos, X. Jin, J. Yang, S. Chen, Z.-L. Yang, D.-Y. Wu, J. M. Feliu, C. T. Williams, Z.-Q. Tian, and J.-F. Li, "In situ Raman spectroscopic evidence for oxygen reduction reaction intermediates at platinum single-crystal surfaces," *Nat. Energy* **4**, 60 (2019).
- <sup>73</sup>R. Chen, Z. Cao, Z. Lyu, M. Xie, Y. Shi, and Y. Xia, "Continuous and scalable synthesis of Pt multipods with enhanced electrocatalytic activity toward the oxygen reduction reaction," *ChemNanoMat* **5**, 599 (2019).
- <sup>74</sup>H. Cheng, Z. Cao, Z. Chen, M. Zhao, M. Xie, Z. Lyu, Z. Zhu, M. Chi, and Y. Xia, "Catalytic system based on sub-2 nm Pt particles and its extraordinary activity and durability for oxygen reduction," *Nano Lett.* **19**, 4997 (2019).
- <sup>75</sup>R. Chen, M. Cao, J. Wang, H. Li, and R. Cao, "Decamethylcucurbit[5]uril based supramolecular assemblies as efficient electrocatalysts for the oxygen reduction reaction," *Chem. Commun.* **55**, 11687 (2019).
- <sup>76</sup>J. Gan, W. Luo, W. Chen, J. Guo, Z. Xiang, B. Chen, F. Yang, Y. Cao, F. Song, X. Duan, and X. Zhou, "Mechanistic understanding of size-dependent oxygen reduction activity and selectivity over Pt/CNT nanocatalysts," *Eur. J. Inorg. Chem.* **2019**, 3210.
- <sup>77</sup>J. Gan, J. Zhang, B. Zhang, W. Chen, D. Niu, Y. Qin, X. Duan, and X. Zhou, "Active sites engineering of Pt/CNT oxygen reduction catalysts by atomic layer deposition," *J. Energy Chem.* **45**, 59 (2020).
- <sup>78</sup>H. R. Litkahi, A. Bahari, and M. P. Gatavi, "Improved oxygen reduction reaction in PEMFCs by functionalized CNTs supported Pt–M (M = Fe, Ni, Fe–Ni) bi- and

- tri-metallic nanoparticles as efficient electrocatalyst," *Int. J. Hydrogen Energy* **45**, 23543 (2020).
- <sup>79</sup>R. Wang, Z. Chang, Z. Fang, T. Xiao, Z. Zhu, B. Ye, C. Xu, and J. Cheng, "Pt nanowire/Ti<sub>3</sub>C<sub>2</sub>T<sub>x</sub>-CNT hybrids catalysts for the high performance oxygen reduction reaction for high temperature PEMFC," *Int. J. Hydrogen Energy* **45**, 28190 (2020).
- <sup>80</sup>C. Xu, C. Fan, X. Zhang, H. Chen, X. Liu, Z. Fu, R. Wang, T. Hong, and J. Cheng, "MXene (Ti<sub>3</sub>C<sub>2</sub>T<sub>x</sub>) and carbon nanotube hybrid-supported platinum catalysts for the high-performance oxygen reduction reaction in PEMFC," *ACS Appl. Mater. Interfaces* **12**, 19539 (2020).
- <sup>81</sup>S. Chung, K. Ham, S. Kang, H. Ju, and J. Lee, "Enhanced corrosion tolerance and highly durable ORR activity by low Pt electrocatalyst on porous structured CNF in PEM fuel cell," *Electrochim. Acta* **348**, 136346 (2020).
- <sup>82</sup>C. He, S. Sankarasubramanian, I. Matanovic, P. Atanassov, and V. Ramani, "Understanding the oxygen reduction reaction activity and oxidative stability of Pt supported on Nb-doped TiO<sub>2</sub>," *ChemSusChem* **12**, 3468 (2019).
- <sup>83</sup>C. Xu, J. Yang, E. Liu, Q. Jia, G. M. Veith, G. Nair, S. DiPietro, K. Sun, J. Chen, P. Pietrasz, Z. Lu, M. Jagner, K. K. Gath, S. Mukerjee, and J. R. Waldecker, "Physical vapor deposition process for engineering Pt based oxygen reduction reaction catalysts on NbO<sub>x</sub> templated carbon support," *J. Power Sources* **451**, 227709 (2020).
- <sup>84</sup>Z. Ma, S. Li, L. Wu, L. Song, G. Jiang, Z. Liang, D. Su, Y. Zhu, R. R. Adzic, J. X. Wang, and Z. Chen, "NbO<sub>x</sub> nano-nail with a Pt head embedded in carbon as a highly active and durable oxygen reduction catalyst," *Nano Energy* **69**, 104455 (2020).
- <sup>85</sup>E. Lee, C. Park, D. W. Lee, G. Lee, H.-Y. Park, J. H. Jang, H.-J. Kim, Y.-E. Sung, Y. Tak, and S. J. Yoo, "Tunable synthesis of N,C-codoped Ti<sup>3+</sup>-enriched titanium oxide support for highly durable PEMFC cathode," *ACS Catal.* **10**, 12080 (2020).
- <sup>86</sup>S. Hussain, H. Erikson, N. Kongi, A. Tarre, P. Ritslaid, A. Kikas, V. Kisand, J. Kozlova, J. Aarik, A. Tamm, V. Sammelselg, and K. Tammeveski, "Platinum sputtered on Nb-doped TiO<sub>2</sub> films prepared by ALD: Highly active and durable carbon-free ORR electrocatalyst," *J. Electrochem. Soc.* **167**, 164505 (2020).
- <sup>87</sup>R. A. MoghadamEsfahani, S. K. Vankova, E. B. Easton, I. I. Ebralidze, and S. Specchia, "A hybrid Pt/NbO/CNTs catalyst with high activity and durability for oxygen reduction reaction in PEMFC," *Renewable Energy* **154**, 913 (2020).
- <sup>88</sup>R. Yue, M. Xia, M. Wang, P. Chen, W. Gong, S. Liao, Z. Li, F. Gao, L. Zhang, and J. Wang, "TiN and TiC as stable and promising supports for oxygen reduction reaction: Theoretical and experimental study," *Appl. Surf. Sci.* **495**, 143620 (2019).
- <sup>89</sup>J. Kim, S.-I. Kim, S. G. Jo, N. E. Hong, B. Ye, S. Lee, H. S. Dow, D. H. Lee, and J. W. Lee, "Enhanced activity and durability of Pt nanoparticles supported on reduced graphene oxide for oxygen reduction catalysts of proton exchange membrane fuel cells," *Catal. Today* **352**, 10 (2020).
- <sup>90</sup>L. Song, Z. Liang, K. Nagamori, H. Igarashi, M. B. Vukmirovic, R. R. Adzic, and K. Sasaki, "Enhancing oxygen reduction performance of Pt monolayer catalysts by Pd(111) nanosheets on WNi substrates," *ACS Catal.* **10**, 4290 (2020).
- <sup>91</sup>M. A. Abdelkareem, T. Wilberforce, K. Elsaid, E. T. Sayed, E. A. M. Abdelghani, and A. G. Olabi, "Transition metal carbides and nitrides as oxygen reduction reaction catalyst or catalyst support in proton exchange membrane fuel cells (PEMFCs)," *Int. J. Hydrogen Energy* (published online, 2020).
- <sup>92</sup>H. Yang, Y. Ko, W. Lee, A. Züttel, and W. Kim, "Nitrogen-doped carbon black supported Pt-M (M = Pd, Fe, Ni) alloy catalysts for oxygen reduction reaction in proton exchange membrane fuel cell," *Mater. Today Energy* **13**, 374 (2019).
- <sup>93</sup>Z. Qiao, S. Hwang, X. Li, C. Wang, W. Samarakoon, S. Karakalos, D. Li, M. Chen, Y. He, M. Wang, Z. Liu, G. Wang, H. Zhou, Z. Feng, D. Su, J. S. Spendlow, and G. Wu, "3D porous graphitic nanocarbon for enhancing the performance and durability of Pt catalysts: A balance between graphitization and hierarchical porosity," *Energy Environ. Sci.* **12**, 2830 (2019).
- <sup>94</sup>S. Ott, A. Orfanidi, H. Schmies, B. Anke, H. N. Nong, J. Hübner, U. Gernert, M. Glicch, M. Lerch, and P. Strasser, "Ionomer distribution control in porous carbon-supported catalyst layers for high-power and low Pt-loaded proton exchange membrane fuel cells," *Nat. Mater.* **19**, 77 (2020).
- <sup>95</sup>E. Padgett, V. Yarlagadda, M. E. Holtz, M. Ko, B. D. A. Levin, R. S. Kukreja, J. M. Ziegelbauer, R. N. Andrews, J. Ilavsky, and A. Kongkanand, "Mitigation of PEM fuel cell catalyst degradation with porous carbon supports," *J. Electrochem. Soc.* **166**, F198 (2019).
- <sup>96</sup>F. Zhou, Y. Yan, S. Guan, W. Guo, M. Sun, and M. Pan, "Solving Nafion poisoning of ORR catalysts with an accessible layer: Designing a nanostructured core-shell Pt/C catalyst via a one-step self-assembly for PEMFC," *Int. J. Energy Res.* **44**, 10155 (2020).
- <sup>97</sup>Y. Nie and Z. Wei, "Surface-confined Pt-based catalysts for strengthening oxygen reduction performance," *Prog. Nat. Sci.* **30**, 796 (2020).
- <sup>98</sup>W. Zhao, Y. Ye, W. Jiang, J. Li, H. Tang, J. Hu, L. Du, Z. Cui, and S. Liao, "Mesoporous carbon confined intermetallic nanoparticles as highly durable electrocatalysts for the oxygen reduction reaction," *J. Mater. Chem. A* **8**, 15822 (2020).
- <sup>99</sup>Y. Li, J. Hart, L. Proffitt, S. Intikhab, S. Chatterjee, M. Taheri, and J. Snyder, "Sequential capacitive deposition of ionic liquids for conformal thin film coatings on oxygen reduction reaction electrocatalysts," *ACS Catal.* **9**, 9311 (2019).
- <sup>100</sup>M. Xiao, J. Zhu, G. Li, N. Li, S. Li, Z. P. Cano, L. Ma, P. Cui, P. Xu, G. Jiang, H. Jin, S. Wang, T. Wu, J. Lu, A. Yu, D. Su, and Z. Chen, "A single-atom iridium heterogeneous catalyst in oxygen reduction reaction," *Angew. Chem.* **131**, 9742 (2019).
- <sup>101</sup>M. Xiao, L. Gao, Y. Wang, X. Wang, J. Zhu, Z. Jin, C. Liu, H. Chen, G. Li, J. Ge, Q. He, Z. Wu, Z. Chen, and W. Xing, "Engineering energy level of metal center: Ru single-atom site for efficient and durable oxygen reduction catalysis," *J. Am. Chem. Soc.* **141**, 19800 (2019).
- <sup>102</sup>Q. Liu, Y. Li, L. Zheng, J. Shang, X. Liu, R. Yu, and J. Shui, "Sequential synthesis and active-site coordination principle of precious metal single-atom catalysts for oxygen reduction reaction and PEM fuel cells," *Adv. Energy Mater.* **10**, 2000689 (2020).
- <sup>103</sup>M. Zhao, J. Holder, Z. Chen, M. Xie, Z. Cao, M. Chi, and Y. Xia, "Facile synthesis of Pt icosahedral nanocrystals with controllable sizes for the evaluation of size-dependent activity toward oxygen reduction," *ChemCatChem* **11**, 2458 (2019).
- <sup>104</sup>W. Lei, M. Li, L. He, X. Meng, Z. Mu, Y. Yu, F. M. Ross, and W. Yang, "A general strategy for bimetallic Pt-based nano-branched structures as highly active and stable oxygen reduction and methanol oxidation bifunctional catalysts," *Nano Res.* **13**, 638 (2020).
- <sup>105</sup>Z. Wang, X. Yao, Y. Kang, L. Miao, D. Xia, and L. Gan, "Structurally ordered low-Pt intermetallic electrocatalysts toward durably high oxygen reduction reaction activity," *Adv. Funct. Mater.* **29**, 1902987 (2019).
- <sup>106</sup>S. Yin, Z. Wang, X. Qian, D. Yang, Y. Xu, X. Li, L. Wang, and H. Wang, "PtM (M = Co, Ni) mesoporous nanotubes as bifunctional electrocatalysts for oxygen reduction and methanol oxidation," *ACS Sustainable Chem. Eng.* **7**, 7960 (2019).
- <sup>107</sup>Q. Liu, L. Du, G. Fu, Z. Cui, Y. Li, D. Dang, X. Gao, Q. Zheng, and J. B. Goodenough, "Structurally ordered Fe<sub>3</sub>Pt nanoparticles on robust nitride support as a high performance catalyst for the oxygen reduction reaction," *Adv. Energy Mater.* **9**, 1803040 (2019).
- <sup>108</sup>D. Wang, G. Hu, P. Yang, X. Pan, H. Xu, L. Liu, J. Zhang, and M. An, "Using DMH as a complexing agent for pulse electrodeposition of platinum nanoparticles towards oxygen reduction reaction," *Ionics* **26**, 3473 (2020).
- <sup>109</sup>B. Ergul-Yilmaz, Z. Yang, M. L. Perry, K. L. More, N. Macauley, R. L. Borup, and T. Karabacak, "Microstructural evolution and ORR activity of nanocolumnar platinum thin films with different mass loadings grown by high pressure sputtering," *J. Electrochem. Soc.* **167**, 134514 (2020).
- <sup>110</sup>L. Mølmen, A. Alexandersson, and P. Leisner, "Surface technology should improve PEM fuel cell performance," *Trans. IMF* **97**, 112 (2019).
- <sup>111</sup>V. Beermann, M. E. Holtz, E. Padgett, J. F. de Araujo, D. A. Muller, and P. Strasser, "Real-time imaging of activation and degradation of carbon supported octahedral Pt-Ni alloy fuel cell catalysts at the nanoscale using in situ electrochemical liquid cell STEM," *Energy Environ. Sci.* **12**, 2476 (2019).
- <sup>112</sup>R. Mom, L. Frevel, J.-J. Velasco-Vélez, M. Plodinec, A. Knop-Gericke, and R. Schlögl, "The oxidation of platinum under wet conditions observed by electrochemical X-ray photoelectron spectroscopy," *J. Am. Chem. Soc.* **141**, 6537 (2019).
- <sup>113</sup>Z. Wu, Y.-Q. Su, E. J. M. Hensen, X. Tian, C. You, and Q. Xu, "Highly stable Pt<sub>3</sub>Ni nanowires tailored with trace Au for the oxygen reduction reaction," *J. Mater. Chem. A* **7**, 26402 (2019).

- <sup>114</sup>Y. Feng, B. Huang, C. Yang, Q. Shao, and X. Huang, "Platinum porous nanosheets with high surface distortion and Pt utilization for enhanced oxygen reduction catalysis," *Adv. Funct. Mater.* **29**, 1904429 (2019).
- <sup>115</sup>F. Kong, M. N. Banis, L. Du, L. Zhang, L. Zhang, J. Li, K. Doyle-Davis, J. Liang, Q. Liu, X. Yang, R. Li, C. Du, G. Yin, and X. Sun, "Highly stable one-dimensional Pt nanowires with modulated structural disorder towards the oxygen reduction reaction," *J. Mater. Chem. A* **7**, 24830 (2019).
- <sup>116</sup>F. Calle-Vallejo, J. Tymoczko, V. Colic, Q. H. Vu, M. D. Pohl, K. Morgenstern, D. Loffreda, P. Sautet, W. Schuhmann, and A. S. Bandarenka, "Finding optimal surface sites on heterogeneous catalysts by counting nearest neighbors," *Science* **350**, 185 (2015).
- <sup>117</sup>C. Wei, R. R. Rao, J. Peng, B. Huang, I. E. L. Stephens, M. Risch, Z. J. Xu, and Y. Shao-Horn, "Recommendation practices and benchmark activity for hydrogen and oxygen electrocatalysis in water splitting and fuel cells," *Adv. Mater.* **31**, 1806296 (2019).
- <sup>118</sup>C. Zalitis, A. Kucernak, X. Lin, and J. Sharman, "Electrochemical measurement of intrinsic oxygen reduction reaction activity at high current densities as a function of particle size for Pt<sub>1-x</sub>Co<sub>x</sub>/C (x = 0, 1, 3) catalysts," *ACS Catal.* **10**, 4361 (2020).
- <sup>119</sup>B. Garlyyev, K. Kratzl, M. Rück, J. Michalička, J. Fichtner, J. M. Macak, T. Kratky, S. Günther, M. Cokoja, A. S. Bandarenka *et al.*, "Optimizing the size of platinum nanoparticles for enhanced mass activity in the electrochemical oxygen reduction reaction," *Angew. Chem., Int. Ed.* **58**, 9596 (2019).
- <sup>120</sup>P. Varathan, S. Akula, P. Moni, and A. K. Sahu, "Natural aloe vera derived Pt supported N-doped porous carbon: A highly durable cathode catalyst of PEM fuel cell," *Int. J. Hydrogen Energy* **45**, 19267 (2020).
- <sup>121</sup>K. Kocher and V. Hacker, "Polyaniline/platinum composite cathode catalysts towards durable polymer electrolyte membrane fuel cells," *ChemistryOpen* **9**, 1109 (2020).
- <sup>122</sup>W.-W. Zhao, P. Bothra, Z. Lu, Y. Li, L.-P. Mei, K. Liu, Z. Zhao, G. Chen, S. Back, S. Siahrostami, A. Kulkarni, J. K. Nørskov, M. Bajdich, and Y. Cui, "Improved oxygen reduction reaction activity of nanostructured CoS<sub>2</sub> through electrochemical tuning," *ACS Appl. Energy Mater.* **2**, 8605 (2019).
- <sup>123</sup>M. E. Kreider, A. Gallo, S. Back, Y. Liu, S. Siahrostami, D. Nordlund, R. Sinclair, J. K. Nørskov, L. A. King, and T. F. Jaramillo, "Precious metal-free nickel nitride catalyst for the oxygen reduction reaction," *ACS Appl. Mater. Interfaces* **11**, 26863 (2019).
- <sup>124</sup>R. Zhong, Y. Wu, Z. Liang, W. Guo, C. Zhi, C. Qu, S. Gao, B. Zhu, H. Zhang, and R. Zou, "Fabricating hierarchically porous and Fe<sub>3</sub>C-embedded nitrogen-rich carbon nanofibers as exceptional electrocatalysts for oxygen reduction," *Carbon* **142**, 115 (2019).
- <sup>125</sup>R. Wu, X. Wan, J. Deng, X. Huang, S. Chen, W. Ding, L. Li, Q. Liao, and Z. Wei, "NaCl protected synthesis of 3D hierarchical metal-free porous nitrogen-doped carbon catalysts for the oxygen reduction reaction in acidic electrolyte," *Chem. Commun.* **55**, 9023 (2019).
- <sup>126</sup>K. Tu, L. Zou, C. Yang, Y. Su, C. Lu, J. Zhu, F. Zhang, C. Ke, and X. Zhuang, "Ionic polyimide derived porous carbon nanosheets as high-efficiency oxygen reduction catalysts for Zn-air batteries," *Chem. Eur. J.* **26**, 6525 (2020).
- <sup>127</sup>R. Kobayashi, T. Ishii, Y. Imashiro, and J. Ozaki, "Synthesis of P- and N-doped carbon catalysts for the oxygen reduction reaction via controlled phosphoric acid treatment of folic acid," *Beilstein J. Nanotechnol.* **10**, 1497 (2019).
- <sup>128</sup>R. Li, F. Liu, Y. Zhang, M. Guo, and D. Liu, "Nitrogen, sulfur Co-doped hierarchically porous carbon as a metal-free electrocatalyst for oxygen reduction and carbon dioxide reduction reaction," *ACS Appl. Mater. Interfaces* **12**, 44578 (2020).
- <sup>129</sup>Y. Wang, S. Wang, R. Li, H. Li, Z. Guo, B. Chen, R. Li, Q. Yao, X. Zhang, H. Chen, Y. Li, K. Qu, and Y. Zheng, "A simple strategy for tridoped porous carbon nanosheet as superior electrocatalyst for bifunctional oxygen reduction and hydrogen evolution reactions," *Carbon* **162**, 586 (2020).
- <sup>130</sup>Y. Deng, B. Chi, J. Li, G. Wang, L. Zheng, X. Shi, Z. Cui, L. Du, S. Liao, K. Zang, J. Luo, Y. Hu, and X. Sun, "Atomic Fe-doped MOF-derived carbon polyhedrons with high active-center density and ultra-high performance toward PEM fuel cells," *Adv. Energy Mater.* **9**, 1802856 (2019).
- <sup>131</sup>L. Gao, M. Xiao, Z. Jin, C. Liu, J. Ge, and W. Xing, "Hydrogen etching induced hierarchical meso/micro-pore structure with increased active density to boost ORR performance of Fe-N-C catalyst," *J. Energy Chem.* **35**, 17 (2019).
- <sup>132</sup>E. Luo, H. Zhang, X. Wang, L. Gao, L. Gong, T. Zhao, Z. Jin, J. Ge, Z. Jiang, C. Liu, and W. Xing, "Single-atom Cr-N<sub>4</sub> sites designed for durable oxygen reduction catalysis in acid media," *Angew. Chem., Int. Ed.* **58**, 12469 (2019).
- <sup>133</sup>K. Liu, Z. Qiao, S. Hwang, Z. Liu, H. Zhang, D. Su, H. Xu, G. Wu, and G. Wang, "Mn- and N-doped carbon as promising catalysts for oxygen reduction reaction: Theoretical prediction and experimental validation," *Appl. Catal. B* **243**, 195 (2019).
- <sup>134</sup>X. Qin, Y. Huang, K. Wang, T. Xu, Y. Wang, P. Liu, Y. Kang, and Y. Zhang, "Ultra-high-loading zinc single-atom catalyst for highly efficient oxygen reduction served as high efficient oxygen reduction reaction catalyst for fuel cells application," *Electrochim. Acta* **297**, 805 (2019).
- <sup>135</sup>J. Li, S. Chen, N. Yang, M. Deng, S. Ibraheem, J. Deng, J. Li, L. Li, and Z. Wei, "Ultra-high-loading zinc single-atom catalyst for highly efficient oxygen reduction in both acidic and alkaline media," *Angew. Chem., Int. Ed.* **58**, 7035 (2019).
- <sup>136</sup>X. X. Wang, D. A. Cullen, Y.-T. Pan, S. Hwang, M. Wang, Z. Feng, J. Wang, M. H. Engelhard, H. Zhang, Y. He *et al.*, "Nitrogen-coordinated single cobalt atom catalysts for oxygen reduction in proton exchange membrane fuel cells," *Adv. Mater.* **30**, 1706758 (2018).
- <sup>137</sup>G. Chen, P. Liu, Z. Liao, F. Sun, Y. He, H. Zhong, T. Zhang, E. Zschech, M. Chen, G. Wu, J. Zhang, and X. Feng, "Zinc-mediated template synthesis of Fe-N-C electrocatalysts with densely accessible Fe-N<sub>x</sub> active sites for efficient oxygen reduction," *Adv. Mater.* **32**, 1907399 (2020).
- <sup>138</sup>X. Wang, Y. Jia, X. Mao, D. Liu, W. He, J. Li, J. Liu, X. Yan, J. Chen, L. Song, A. Du, and X. Yao, "Edge-rich Fe-N<sub>4</sub> active sites in defective carbon for oxygen reduction catalysis," *Adv. Mater.* **32**, 2000966 (2020).
- <sup>139</sup>Y. Deng, X. Tian, B. Chi, Q. Wang, W. Ni, Y. Gao, Z. Liu, J. Luo, C. Lin, L. Ling, F. Cheng, Y. Zhang, S. Liao, and S. Zhang, "Hierarchically open-porous carbon networks enriched with exclusive Fe-N<sub>x</sub> active sites as efficient oxygen reduction catalysts towards acidic H<sub>2</sub>-O<sub>2</sub> PEM fuel cell and alkaline Zn-air battery," *Chem. Eng. J.* **390**, 124479 (2020).
- <sup>140</sup>Y. Deng, B. Chi, X. Tian, Z. Cui, E. Liu, Q. Jia, W. Fan, G. Wang, D. Dang, M. Li, K. Zang, J. Luo, Y. Hu, S. Liao, X. Sun, and S. Mukerjee, "g-C<sub>3</sub>N<sub>4</sub> promoted MOF derived hollow carbon nanopolyhedra doped with high density/fraction of single Fe atoms as an ultra-high performance non-precious catalyst towards acidic ORR and PEM fuel cells," *J. Mater. Chem. A* **7**, 5020 (2019).
- <sup>141</sup>M. Karuppannan, J. E. Park, H. E. Bae, Y.-H. Cho, and O. J. Kwon, "A nitrogen and fluorine enriched Fe/Fe<sub>3</sub>C@C oxygen reduction reaction electrocatalyst for anion/proton exchange membrane fuel cells," *Nanoscale* **12**, 2542 (2020).
- <sup>142</sup>X. Wan, X. Liu, Y. Li, R. Yu, L. Zheng, W. Yan, H. Wang, M. Xu, and J. Shui, "Fe-N-C electrocatalyst with dense active sites and efficient mass transport for high-performance proton exchange membrane fuel cells," *Nat. Catal.* **2**, 259 (2019).
- <sup>143</sup>N. Zhang, T. Zhou, M. Chen, H. Feng, R. Yuan, C. Zhong, W. Yan, Y. Tian, X. Wu, W. Chu, C. Wu, and Y. Xie, "High-purity pyrrole-type FeN<sub>4</sub> sites as a superior oxygen reduction electrocatalyst," *Energy Environ. Sci.* **13**, 111 (2020).
- <sup>144</sup>K. Kumar, L. Dubau, M. Mermoux, J. Li, A. Zitolo, J. Nelayah, F. Jaouen, and F. Maillard, "On the influence of oxygen on the degradation of Fe-N-C catalysts," *Angew. Chem., Int. Ed.* **59**, 3235 (2020).
- <sup>145</sup>S. Chen, N. Zhang, C. W. Narváez Villarrubia, X. Huang, L. Xie, X. Wang, X. Kong, H. Xu, G. Wu, J. Zeng, and H.-L. Wang, "Single Fe atoms anchored by short-range ordered nanographene boost oxygen reduction reaction in acidic media," *Nano Energy* **66**, 104164 (2019).
- <sup>146</sup>Y. Mun, S. Lee, K. Kim, S. Kim, S. Lee, J. W. Han, and J. Lee, "Versatile strategy for tuning ORR activity of a single Fe-N<sub>4</sub> site by controlling electron-withdrawing/donating properties of a carbon plane," *J. Am. Chem. Soc.* **141**, 6254 (2019).
- <sup>147</sup>K. Artyushkova, S. Rojas-Carbonell, C. Santoro, E. Weiler, A. Serov, R. Awais, R. R. Gokhale, and P. Atanassov, "Correlation between synthesis and performance of Fe-based PGM-free catalysts in acidic and alkaline media: Evolution of surface chemistry and morphology," *ACS Appl. Energy Mater.* **2**, 5406 (2019).
- <sup>148</sup>X. Ao, W. Zhang, Z. Li, J.-G. Li, L. Soule, X. Huang, W.-H. Chiang, H. M. Chen, C. Wang, M. Liu, and X. C. Zeng, "Markedly enhanced oxygen reduction activity of single-atom Fe catalysts via integration with Fe nanoclusters," *ACS Nano* **13**, 11853 (2019).

- <sup>149</sup>G. Wu and Y. Nie, "N, S codoped iron-carbon-based electrocatalyst for oxygen reduction reaction via salt recrystallization strategy," *Chem. Lett.* **50**, 124 (2021).
- <sup>150</sup>D. Liu, B. Wang, H. Li, S. Huang, M. Liu, J. Wang, Q. Wang, J. Zhang, and Y. Zhao, "Distinguished Zn,Co-N<sub>x</sub>-C-S<sub>y</sub> active sites confined in dendritic carbon for highly efficient oxygen reduction reaction and flexible Zn-air batteries," *Nano Energy* **58**, 277 (2019).
- <sup>151</sup>H. Jin, H. Zhou, D. He, Z. Wang, Q. Wu, Q. Liang, S. Liu, and S. Mu, "MOF-derived 3D Fe-N-S Co-doped carbon matrix/nanotube nanocomposites with advanced oxygen reduction activity and stability in both acidic and alkaline media," *Appl. Catal. B* **250**, 143 (2019).
- <sup>152</sup>J. Liu, L. Xu, Y. Deng, X. Zhu, J. Deng, J. Lian, J. Wu, J. Qian, H. Xu, S. Yuan, H. Li, and P. M. Ajayan, "Metallic cobalt nanoparticles embedded in sulfur and nitrogen Co-doped rambutan-like nanocarbons for the oxygen reduction reaction under both acidic and alkaline conditions," *J. Mater. Chem. A*, **7**, 14291 (2019).
- <sup>153</sup>X. Yang, Y. Wang, G. Zhang, L. Du, L. Yang, M. Markiewicz, J. Choi, R. Chenitz, and S. Sun, "SiO<sub>2</sub>-Fe/N/C catalyst with enhanced mass transport in PEM fuel cells," *Appl. Catal. B* **264**, 118523 (2020).
- <sup>154</sup>J.-C. Li, F. Xiao, H. Zhong, T. Li, M. Xu, L. Ma, M. Cheng, D. Liu, S. Feng, Q. Shi, H.-M. Cheng, C. Liu, D. Du, S. P. Beckman, X. Pan, Y. Lin, and M. Shao, "Secondary-atom-assisted synthesis of single iron atoms anchored on N-doped carbon nanowires for oxygen reduction reaction," *ACS Catal.* **9**, 5929 (2019).
- <sup>155</sup>Y. Luo, J. Zhang, J. Chen, Y. Chen, Z. Li, J. Shi, G. Wang, and R. Wang, "Dual-temple construction of iron-nitrogen-codoped hierarchically porous carbon electrocatalyst for oxygen reduction reaction," *Energy Fuels* **34**, 16720 (2020).
- <sup>156</sup>F. Razmjooei, J.-H. Yu, H.-Y. Lee, B.-J. Lee, K. P. Singh, T.-H. Kang, H.-J. Kim, and J.-S. Yu, "Single-atom iron-based electrocatalysts for high-temperature polymer electrolyte membrane fuel cell: Organometallic precursor and pore texture tailoring," *ACS Appl. Energy Mater.* **3**, 11164 (2020).
- <sup>157</sup>L. Jiao, R. Zhang, G. Wan, W. Yang, X. Wan, H. Zhou, J. Shui, S.-H. Yu, and H.-L. Jiang, "Nanocasting SiO<sub>2</sub> into metal-organic frame works imparts dual protection to high-loading Fe single-atom electrocatalysts," *Nat. Commun.* **11**, 2831 (2020).
- <sup>158</sup>J. Li, H. Zhang, W. Samarakoon, W. Shan, D. A. Cullen, S. Karakalos, M. Chen, D. Gu, K. L. More, G. Wang, Z. Feng, Z. Wang, and G. Wu, "Thermally driven structure and performance evolution of atomically dispersed FeN<sub>4</sub> sites for oxygen reduction," *Angew. Chem., Int. Ed.* **58**, 18971 (2019).
- <sup>159</sup>X. Shi, Z. Pu, B. Chi, M. Liu, S. Yu, L. Zheng, L. Yang, T. Shu, and S. Liao, "Nitrogen and atomic Fe dual-doped porous carbon nanocubes as superior electrocatalysts for acidic H<sub>2</sub>-O<sub>2</sub> PEMFC and alkaline Zn-air battery," *J. Energy Chem.* **59**, 388 (2021).
- <sup>160</sup>R. Wang, Y. Yang, Y. Zhao, L. Yang, P. Yin, J. Mao, and T. Ling, "Multiscale structural engineering of atomically dispersed FeN<sub>4</sub> electrocatalyst for proton exchange membrane fuel cells," *J. Energy Chem.* **58**, 629 (2021).
- <sup>161</sup>R. Wang, P. Zhang, Y. Wang, Y. Wang, K. Zaghbi, and Z. Zhou, "ZIF-derived Co-N-C ORR catalyst with high performance in proton exchange membrane fuel cells," *Prog. Nat. Sci.* **30**, 855 (2020).
- <sup>162</sup>Y. Qian, Q. Liu, E. Sarnello, C. Tang, M. Chng, J. Shui, T. Li, S. J. Pennycook, M. Han, and D. Zhao, "MOF-derived carbon networks with atomically dispersed Fe-N<sub>x</sub> sites for oxygen reduction reaction catalysis in acidic media," *ACS Mater. Lett.* **1**, 37 (2019).
- <sup>163</sup>F. Xiao, G.-L. Xu, C.-J. Sun, M. Xu, W. Wen, Q. Wang, M. Gu, S. Zhu, Y. Li, Z. Wei, X. Pan, J. Wang, K. Amine, and M. Shao, "Nitrogen-coordinated single iron atom catalysts derived from metal organic frameworks for oxygen reduction reaction," *Nano Energy* **61**, 60 (2019).
- <sup>164</sup>Z. Zhu, H. Yin, Y. Wang, C. H. Chuang, L. Xing, M. Dong, Y. R. Lu, G. Casillas-García, Y. Zheng, S. Chen, Y. Dou, P. Liu, Q. Cheng, and H. Zhao, "Coexisting single-atomic Fe and Ni sites on hierarchically ordered porous carbon as a highly efficient ORR electrocatalyst," *Adv. Mater.* **32**, 2004670 (2020).
- <sup>165</sup>X. Zhang, Y. B. Mollamahale, D. Lyu, L. Liang, F. Yu, M. Qing, Y. Du, X. Zhang, Z. Q. Tian, and P. K. Shen, "Molecular-level design of Fe-N-C catalysts derived from Fe-dual pyridine coordination complexes for highly efficient oxygen reduction," *J. Catal.* **372**, 245 (2019).
- <sup>166</sup>H. Wang, F. X. Yin, N. Liu, R. H. Kou, X. B. He, C. J. Sun, B. H. Chen, D. J. Liu, and H. Q. Yin, "Engineering Fe-Fe<sub>3</sub>C@Fe-N-C active sites and hybrid structures from dual metal-organic frameworks for oxygen reduction reaction in H<sub>2</sub>-O<sub>2</sub> fuel cell and Li-O<sub>2</sub> battery," *Adv. Funct. Mater.* **29**, 1901531 (2019).
- <sup>167</sup>Z. Sun, J. Lin, K. Hou, L. Guan, and H. Zhan, "Pore engineering of an Fe-N-C electrocatalyst to enhance the performance for the oxygen reduction reaction by adding g-C<sub>3</sub>N<sub>4</sub> into polyaniline and cyanamide as a precursor," *J. Mater. Chem. A* **8**, 7273 (2020).
- <sup>168</sup>L. Zheng, S. Yu, X. Lu, W. Fan, B. Chi, Y. Ye, X. Shi, J. Zheng, X. Li, and S. Liao, "Two-dimensional bimetallic Zn/Fe-metal-organic framework (MOF)-derived porous carbon nanosheets with a high density of single/paired Fe atoms as high-performance oxygen reduction catalysts," *ACS Appl. Mater. Interfaces* **12**, 13878 (2020).
- <sup>169</sup>X. Fu, N. Li, B. Ren, G. Jiang, Y. Liu, F. M. Hassan, D. su, J. Zhu, L. Yang, Z. Bai, Z. P. Cano, A. Yu, and Z. Chen, "Tailoring FeN<sub>4</sub> sites with edge enrichment for boosted oxygen reduction performance in proton exchange membrane fuel cell," *Adv. Energy Mater.* **9**, 1803737 (2019).
- <sup>170</sup>K. Wang, H. Chen, X. Zhang, Y. Tong, S. Song, P. Tsiakaras, and Y. Wang, "Iron oxide/graphitic carbon core-shell nanoparticles embedded in ordered mesoporous N-doped carbon matrix as an efficient cathode catalyst for PEMFC," *Appl. Catal. B* **264**, 118468 (2020).
- <sup>171</sup>Y. Wang and S. Berthon-Fabry, "One-pot synthesis of Fe-N-containing carbon aerogel for oxygen reduction reaction," *Electrocatalysis* **12**, 78 (2021).
- <sup>172</sup>Z. Yang, Y. Wang, M. Zhu, Z. Li, W. Chen, W. Wei, T. Yuan, Y. Qu, Q. Xu, C. Zhao, X. Wang, P. Li, Y. Li, Y. Wu, and Y. Li, "Boosting oxygen reduction catalysis with Fe-N<sub>4</sub> sites decorated porous carbons toward fuel cells," *ACS Catal.* **9**, 2158 (2019).
- <sup>173</sup>J.-C. Li, M. Cheng, T. Li, L. Ma, X. Ruan, D. Liu, H.-M. Cheng, C. Liu, D. Du, Z. Wei, Y. Lin, and M. Shao, "Carbon nanotube-linked hollow carbon nanospheres doped with iron and nitrogen as single-atom catalysts for the oxygen reduction reaction in acidic solutions," *J. Mater. Chem. A* **7**, 14478 (2019).
- <sup>174</sup>D. Liu, J.-C. Li, Q. Shi, S. Feng, Z. Lyu, S. Ding, L. Hao, Q. Zhang, C. Wang, M. Xu, T. Li, E. Sarnello, D. Du, and Y. Lin, "Atomically isolated iron atom anchored on carbon nanotubes for oxygen reduction reaction," *ACS Appl. Mater. Interfaces* **11**, 39820 (2019).
- <sup>175</sup>D. Liu, J. C. Li, S. Ding, Z. Lyu, S. Feng, H. Tian, C. Huan, M. Xu, T. Li, D. Du, P. Liu, M. Shao, and Y. Lin, "2D single-atom catalyst with optimized iron sites produced by thermal melting of metal-organic frameworks for oxygen reduction reaction," *Small Methods* **4**, 1900827 (2020).
- <sup>176</sup>Y. He, S. Hwang, D. A. Cullen, M. A. Uddin, L. Langhorst, B. Li, S. Karakalos, A. J. Kropf, E. C. Wegener, J. Sokolowski, M. Chen, D. Myers, D. Su, K. L. More, G. Wang, S. Litster, and G. Wu, "Highly active atomically dispersed CoN<sub>4</sub> fuel cellcathode catalysts derived from surfactant-assisted MOFs: Carbon-shell confinement strategy," *Energy Environ. Sci.* **12**, 250 (2019).
- <sup>177</sup>C.-L. Zhang, B.-R. Lu, F.-H. Cao, Z.-Y. Wu, W. Zhang, H.-P. Cong, and S.-H. Yu, "Electrospun metal-organic framework nanoparticle fibers and their derived electrocatalysts for oxygen reduction reaction," *Nano Energy* **55**, 226 (2019).
- <sup>178</sup>X. Wen, L. Bai, M. Li, and J. Guan, "Atomically dispersed cobalt- and nitrogen-codoped graphene toward bifunctional catalysis of oxygen reduction and hydrogen evolution reactions," *ACS Sustainable Chem. Eng.* **7**, 9249 (2019).
- <sup>179</sup>Y. Zhou, W. Yang, W. Utetiwo, Y.-m. Lian, X. Yin, L. Zhou, P. Yu, R. Chen, and S. Sun, "Revealing of active sites and catalytic mechanism in N-coordinated Fe, Ni dual-doped carbon with superior acidic oxygen reduction than single-atom catalyst," *J. Phys. Chem. Lett.* **11**, 1404 (2020).
- <sup>180</sup>H. Zhang, W. Xia, H. Shen, W. Guo, Z. Liang, K. Zhang, Y. Wu, B. Zhu, and R. Zou, "Antiperovskite intermetallic nanoparticles for enhanced oxygen reduction," *Angew. Chem., Int. Ed.* **59**, 1871 (2020).
- <sup>181</sup>H. Yoon, S. Lee, S. Oh, H. Park, S. Choi, and M. Oh, "Synthesis of bimetallic conductive 2D metal-organic framework (Co<sub>x</sub>Ni<sub>y</sub>-CAT) and its mass production: Enhanced electrochemical oxygen reduction activity," *Small* **15**, 1805232 (2019).
- <sup>182</sup>J. Zang, F. Wang, Q. Cheng, G. Wang, L. Ma, C. Chen, L. Yang, Z. Zou, D. Xie, and H. Yang, "Cobalt/zinc dual-sites coordinated with nitrogen in nanofibers enabling efficient and durable oxygen reduction reaction in acidic fuel cells," *J. Mater. Chem. A* **8**, 3686 (2020).
- <sup>183</sup>Z. Lu, B. Wang, Y. Hu, W. Liu, Y. Zhao, R. Yang, Z. Li, J. Luo, B. Chi, Z. Jiang, M. Li, S. Mu, S. Liao, J. Zhang, and X. Sun, "An isolated zinc-cobalt atomic pair



- for highly active and durable oxygen reduction,” *Angew. Chem., Int. Ed.* **131**, 2648 (2019).
- <sup>184</sup>W. Ye, S. Chen, Y. Lin, L. Yang, S. Chen, X. Zheng, Z. Qi, C. Wang, R. Long, M. Chen, J. Zhu, P. Gao, L. Song, J. Jiang, and Y. Xiong, “Precisely tuning the number of Fe atoms in clusters on N-doped carbon toward acidic oxygen reduction reaction,” *Chem* **5**, 2865 (2019).
- <sup>185</sup>N. Zhang, T. Zhou, J. Ge, Y. Lin, Z. Du, C. Zhong, W. Wang, Q. Jiao, R. Yuan, Y. Tian, W. Chu, C. Wu, and Y. Xie, “High-density planar-like Fe<sub>2</sub>N<sub>6</sub> structure catalyzes efficient oxygen reduction,” *Matter* **3**, 509 (2020).
- <sup>186</sup>G. Bae, M. W. Chung, S. G. Ji, F. Jaouen, and C. H. Choi, “pH effect on the H<sub>2</sub>O<sub>2</sub>-induced deactivation of Fe–N–C catalysts,” *ACS Catal.* **10**, 8485 (2020).
- <sup>187</sup>T. Reshetenko, V. Laue, U. Krewer, and K. Artyushkova, “Study of degradation and spatial performance of low Pt-loaded proton exchange membrane fuel cells under exposure to sulfur dioxide in an oxidant stream,” *J. Power Sources* **458**, 228032 (2020).
- <sup>188</sup>L. Wang, S. Bliznakov, R. Isseroff, Y. Zhou, X. Zuo, A. Raut, W. Wang, M. Cuiffo, T. Kim, and M. H. Rafailovich, “Enhancing proton exchange membrane fuel cell performance via graphene oxide surface synergy,” *Appl. Energy* **261**, 114277 (2020).
- <sup>189</sup>E. Daş, S. A. Gürsel, and A. B. Yurtcan, “Pt-alloy decorated graphene as an efficient electrocatalyst for PEM fuel cell reactions,” *J. Supercrit. Fluids* **165**, 104962 (2020).
- <sup>190</sup>P. Satjaritanun and I. V. Zenyuk, “Water management strategies for PGM-free catalyst layers for polymer electrolyte fuel cells,” *Curr. Opin. Electrochem.* **25**, 100622 (2021).
- <sup>191</sup>J. Liu, M. R. Talarposhti, T. Asset, D. C. Sabarirajan, D. Y. Parkinson, P. Atanassov, and I. V. Zenyuk, “Understanding the role of interfaces for water management in platinum group metal-free electrodes in polymer electrolyte fuel cells,” *ACS Appl. Energy Mater.* **2**, 3542 (2019).
- <sup>192</sup>A. Baricci, A. Bisello, A. Serov, M. Odgaard, P. Atanassov, and A. Casalegno, “Analysis of the effect of catalyst layer thickness on the performance and durability of platinum group metal-free catalysts for polymer electrolyte membrane fuel cells,” *Sustainable Energy Fuels* **3**, 3375 (2019).
- <sup>193</sup>T. Reshetenko, G. Randolf, M. Odgaard, B. Zulevi, A. Serov, and A. Kulikovskiy, “The effect of proton conductivity of Fe–N–C–based cathode on PEM fuel cell performance,” *J. Electrochem. Soc.* **167**, 084501 (2020).
- <sup>194</sup>D. Seeberger, D. McLaughlin, P. Hauenstein, and S. Thiele, “Bipolar-interface fuel cells—An underestimated membrane electrode assembly concept for PGM free ORR catalysts,” *Sustainable Energy Fuels* **4**, 2508 (2020).
- <sup>195</sup>A. Lotrič, M. Sekavčnik, I. Kuštrin, and M. Mori, “Life-cycle assessment of hydrogen technologies with the focus on EU critical raw materials and end-of-life strategies,” *Int. J. Hydrogen Energy* **46**, 10143 (2021).
- <sup>196</sup>C. Hagelūken, “Recycling the platinum group metals: A european perspective,” *Platinum Met. Rev.* **56**, 29 (2012).
- <sup>197</sup>R. Sharma, K. R. Nielsen, P. B. Lund, S. B. Simonsen, L. Grahl-Madsen, and S. M. Andersen, “Sustainable platinum recycling through electrochemical dissolution of platinum nanoparticles from fuel cell electrodes,” *ChemElectroChem* **6**, 4471 (2019).
- <sup>198</sup>R. Sharma, S. J. Andreasen, J. Chamier, and S. M. Andersen, “Pt/C electrocatalyst synthesis from recycling of the spent PEMFC membrane electrode assembly: A closed loop circular economy,” *J. Electrochem. Soc.* **166**, F963 (2019).